

UNIVERSIDADE FEDERAL DO RIO GRANDE DO SUL - UFRGS
ESCOLA DE ENGENHARIA
DEPARTAMENTO DE ENGENHARIA ELÉTRICA

EDUARDO LAZZAROTTO FABBRIS

**Radiation Fault Detection System for SEE
in a Mixed-signal Programmable SOC**

PORTE ALEGRE
2025

UNIVERSIDADE FEDERAL DO RIO GRANDE DO SUL - UFRGS
ESCOLA DE ENGENHARIA
DEPARTAMENTO DE ENGENHARIA ELÉTRICA

EDUARDO LAZZAROTTO FABBRIS

**Radiation Fault Detection System for SEE
in a Mixed-signal Programmable SOC**

Graduation thesis, presented to the Department of Electrical Engineering of the School of Engineering of the Universidade Federal do Rio Grande do Sul, as a partial requirement for obtaining the degree of Electrical Engineer

Advisor: Prof. Dr. Tiago Roberto Balen

PORTO ALEGRE
2025

Abstract

Detecting the possible errors that radiation may cause to a device is the first step in understanding its consequences and being able to better mitigate its effects. This work addresses the challenges of Single Event Effects in microelectronics and proposes a soft error identification system for a mixed-signal circuit operating in a Programmable System on Chip (PSoC 6), allowing future works to evaluate the susceptibility of this Commercial Off-The-Shelf (COTS) device through physical irradiation tests. This identification system, also referred to as monitoring system throughout this work, is composed of three elements: the PSoC 6, which runs an error identification routine and will be exposed to radiation; an auxiliary device that acts as an external watchdog, constantly evaluating the status of the device under test (PSoC 6); and a computer program, the PSoC 6 Monitor, responsible for managing the entire system and storing a record of the radiation experiment being performed. The proposed system was validated by emulating known effects already observed in prior works, where an older version of the same programmable device (PSoC 5) was studied. The error simulation was performed via software by using an integrated debug platform from the monitoring program, biasing the device under test to respond as though it had been targeted by an energetic particle.

Keywords: Programmable System on Chip (PSOC), PSoC 6, Radiation effects, Monitoring system, Error identification, Single Event Effects (SEE), Soft errors, Mixed-signal

Resumo

Detectar os possíveis erros que a radiação pode causar em um dispositivo é o primeiro passo para entender as suas consequências e ser capaz de melhor mitigar os seus efeitos. Este trabalho aborda os desafios dos Efeitos Singulares (Single Event Effects) em microeletrônica e propõe um sistema de identificação de erros suaves (soft errors) para um circuito de sinais mistos operando em um Sistema Programável em Chip (PSoC 6), permitindo que trabalhos futuros avaliem a suscetibilidade deste dispositivo disponível comercialmente (COTS) por meio de testes físicos de irradiação. Este sistema de identificação, também denominado sistema de monitoramento ao longo do trabalho, é composto por três elementos: o PSoC 6, que executa uma rotina de identificação de erros e será exposto à radiação; um dispositivo auxiliar que atua como um watchdog externo, avaliando constantemente o status do dispositivo sob teste (PSoC 6); e um programa de computador, o PSoC 6 Monitor, responsável por gerenciar todo o sistema e armazenar um registro do experimento de radiação sendo realizado. O sistema proposto foi validado pela emulação de efeitos conhecidos já observados em trabalhos anteriores, onde uma versão mais antiga do mesmo dispositivo programável (PSoC 5) foi estudada. A simulação de erros foi realizada via software utilizando uma plataforma de depuração integrada ao programa de monitoramento, estimulando o dispositivo sob teste para responder como se tivesse sido atingido por uma partícula energética.

Palavras-chaves: Sistema Programável em Chip (PSOC), PSoC 6, Efeitos da radiação, Sistema de monitoramento, Identificação de Erros, Efeitos Singulares (SEE), Erros suaves, Sinal misto

List of Figures

Figure 2.1 - Different outcomes for a particle interaction on a slab of matter.	13
Figure 2.2 - The electromagnetic spectrum, categorized by the photon energy in eV, as well as wavelength and frequency.	14
Figure 2.3 - The three main energy transfer processes of a photon with matter.	15
Figure 2.4 - The three main energy transfer processes of an electron with matter.	16
Figure 2.5 - Inelastic neutron collision nuclear reactions.....	17
Figure 2.6 - Cartoon depicting the different radiation sources found in space: radiation belts, solar flares and galactic cosmic radiation.	19
Figure 2.7 - Orbit types for a satellite based on altitude, inclination and shape.	20
Figure 2.8 - Cross-section cutaway of the Van Allen belts surrounding Earth. Blue and green represent lower fluxes, and orange and red correspond to high particle flux.	22
Figure 2.9 - Particle shower created in the upper atmosphere by cosmic ray protons interaction with nitrogen or oxygen.....	25
Figure 2.10 - Variation of neutron flux with altitude. Comparison between a high-elevation city and commercial flight altitude.	26
Figure 2.11 - Examples of specialized radiation environments.....	27
Figure 2.12 - The process responsible for the Total Ionizing Dose effect in a MOS device.	31
Figure 2.13 - Fractional Yield x Electric Field for different radiation types.	32
Figure 2.14 - Single Event Effects classification diagram.	34
Figure 2.15 - Phases of charge collection and resulting transient current caused by the passage of a high energy ion.....	35
Figure 2.16 - SEE-induced current pulse at a CMOS inverter translated into a voltage pulse.	36
Figure 2.17 - Examples of different masking types in combinational logic circuits..	38
Figure 2.18 - SEE-induced bit-flip in a memory element.....	39
Figure 3.1 - Programmable system on chip example	42
Figure 3.2 - PSoC 6 mounted in the development kit Infineon CY8CPROTO-063-BLE	43

Figure 3.3 - Basic SAR architecture	44
Figure 3.4 - Simple binary-weighted current-switching DAC	44
Figure 3.5 - SEU corruption of a buffer descriptor	45
Figure 3.6 - PSoC 6 features.....	46
Figure 4.1 - Monitoring system connection schematic.	47
Figure 4.2 - Experimental monitoring setup.....	48
Figure 4.3 - Scheme of the fault detection system inside the main device.....	49
Figure 4.4 - Main device processor interrupt routine flow diagram.	51
Figure 4.5 - Block diagram in PSoC Creator.	52
Figure 4.6 - External watchdog routine flow diagram.	53
Figure 4.7 - PSoC 6 Monitor initial menu.	54
Figure 4.8 - PSoC 6 Monitor serial port configuration.	55
Figure 4.9 - PSoC 6 Monitor monitoring menu.	56
Figure 4.10 -Monitoring software routine flow diagram.	56
Figure 4.11 -Information stored in a log file.	59
Figure 4.12 -PSoC 6 Monitor session aborted.	60
Figure 5.1 - PSoC 6 Monitor debug menu.	62
Figure 5.2 - Oscilloscope at the DAC output.	63
Figure 5.3 - PSoC 5 SEFI example.	63
Figure 5.4 - PSoC 5 SEU example.	64
Figure 5.5 - PSoC 6 SEFI emulation through debug platform.	65
Figure 5.6 - PSoC 6 SEU emulation through debug platform.....	66

List of Tables

Table 4.1 - Buffer packet format.....	57
Table 4.2 - Packet header fields.....	57
Table 4.3 - Packet payload fields.	58
Table 4.4 - Error type descriptor register.....	58

Acronyms List

ADC	Analog-to-Digital Converter
ASIC	Application-Specific Integrated Circuit
COTS	Commercial Off-The-Shelf
DAC	Digital-to-Analog Converter
DD	Displacement Damage
DMA	Direct Memory Access
DRAM	Dynamic Random Access Memory
EMP	Electromagnetic Pulse
FPGA	Field-Programmable Gate Array
GCR	Galactic Cosmic Ray
GR	Geomagnetic Rigidity
IC	Integrated Circuit
LET	Linear Energy Transfer
LUT	Look-Up Table
MCU	Microcontroller Unit
MOS	Metal-Oxide-Semiconductor
NASA	National Aeronautics and Space Administration
PSOC	Programmable System on Chip
SAA	South Atlantic Anomaly
SEE	Single Event Effects
SEFI	Single Event Functional Interrupt
SET	Single Event Transient
SEU	Single Event Upset
SRAM	Static Random Access Memory
TID	Total Ionizing Dose
ULA	Ultra-Low-Alpha

Table of Contents

1	Introduction.....	10
2	Radiation in Electronics.....	12
2.1	What is Radiation?	12
2.2	Radiation Particles	13
2.2.1	Photons	13
2.2.2	Electrons	15
2.2.3	Neutrons.....	16
2.2.4	Protons	18
2.2.5	Ions	18
2.3	Radiation Environments	18
2.3.1	Space Environment.....	18
2.3.1.1	Solar radiation.....	20
2.3.1.2	Galactic cosmic rays.....	21
2.3.1.3	Radiation Belts	21
2.3.2	Terrestrial Environment	23
2.3.3	Alpha particles.....	23
2.3.4	Neutrons.....	24
2.3.5	Specialized Environment	27
2.3.6	Medical field	27
2.3.7	Industrial field	28
2.3.8	Military field	29
2.4	Radiation Effects	29
2.4.1	Total Ionizing Dose	30
2.4.2	Displacement Damage	33
2.4.3	Single Event Effects.....	33
2.4.4	Dose Rate Effects.....	40

2.5	Radiation Effects Mitigation.....	40
3	Programmable System on Chip.....	42
3.1	PSoC 6.....	43
3.1.1	Analog to Digital Converter	44
3.1.2	Digital to Analog Converter	44
3.1.3	Direct Memory Access.....	45
3.1.4	Universal Asynchronous Receiver-Transmitter	45
4	Design Under Test.....	47
4.1	Monitoring System	47
4.2	Main Device	48
4.3	External Watchdog	52
4.4	Monitoring Software	54
5	Design Validation.....	62
6	Conclusion	68
	References.....	70

1 Introduction

The increased capability of electronics has also introduced new concerns, as the higher density of transistors, lower power supply and reduced dimensions make a device more susceptible to Single Event Effects. Whether or not radiation effects pose a reliability risk for electronics depends on the type of application. Critical mission applications related to human, economic and environmental impacts are of high importance and often have significant consequences if they do not succeed.

Radiation sources can be encountered in three primary environments: the space, where the functionality of satellites, probes and shuttles communication systems will be directly influenced by radiation coming from the Sun and other parts of the galaxy; the terrestrial environment, in which most electronic systems operate and aviation plays an important role; and specialized environments, such as medical, industrial and military sites, where man-made radiation commonly dominates over natural radiation.

Nuclear power plants have recently attracted major companies, driven by the surge in Artificial Intelligence. These plants will also support the future electrical power grid, as electric cars are gradually becoming more popular and new governments offer incentives for purchasing these new vehicles. Special devices are required for operation in these industrial environments, as gauges, liquid-level detectors and others instruments are directly exposed to radiation.

The first evidence of radiation effects in space occurred in 1962 with the Telstar satellite (Balen, 2010) [1]. Microelectronics in space are of extreme importance, and their correct functionality will enable future space programs, like NASA's Artemis, to reestablish the human presence on the Moon, laying a foundation to send humans to Mars in the future.

Historical data from soft errors in commercial systems is usually hard to come by, partly because it is hard to trace an error back to an energetic particle strike, and partly because companies are not comfortable in sharing problems with their equipment. In 2004, Cypress Semiconductor, the company that fabricates the studied device (PSoC 6), reported a number of incidents related to soft errors (Mukherjee, 2008) [2].

The objective of this work is to develop a fault monitoring system in order to identify errors due to radiation. This thesis is organized as follows: Chapter 2 reviews the radiation types and their interaction with matter, also covering its effects on electronics. Chapter 3 presents the studied device from Cypress (PSoC 6) and compile some of its available features.

Chapter 4 describes the proposed monitoring system and explains some of the design choices. Chapter 5 shows the experimental results validating the system by software emulation. Chapter 6 summarizes this work's contributions.

2 Radiation in Electronics

A major issue for microelectronics is the excess charge created by energy absorbed from radiation, originating transients or permanent charge reallocation that can lead to parametric and functional failures (Baumann and Kruckmeyer, 2019) [3].

This chapter aims to discuss the fundamentals of radiation and its effects in microelectronics. The initial sections are dedicated to providing a background about the radiation interaction with matter and the typical environments they are found, focusing in the radiation type responsible for the studied effects in this work. After a briefly physics review, the last sections present the consequences of the radiation interaction with a semiconductor, and how it can affect analog and digital circuits.

The term “ionizing radiation” is commonly heard in medical environments, meaning the radiation energy capable of breaking a covalent bond from the DNA of a molecule or the radiation energy capable of ionizing a molecule. This term can also be seen in electronics, referring to the radiation energy sufficient to interact with a device’s material – usually silicon – structure, removing electrons from the atoms and molecules, thereby damaging its properties. In contrast, non-ionizing radiation does not carry enough energy to ionize atoms and molecules, only to excite them.

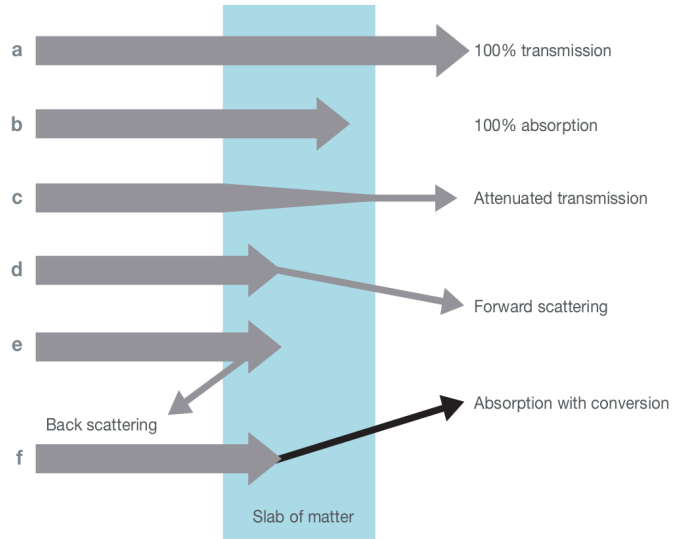
2.1 What is Radiation?

Radiation is energy transport from one location to another. Thinking in terms of Classical Physics, it is typically divided into two types: Particle Radiation, when energy is carried by ions or sub-atomic particles; and Electromagnetic Radiation, when energy is transferred through electromagnetic waves. This distinction is not wrong, although throughout this chapter it will be considered the Quantum Mechanics point of view, and treat radiation as energy transported by different particles that exhibit particle-like and wave-like behavior based on the Wave-particle Duality (French and Taylor, 1978) [4], first introduced in 1905 by Albert Einstein with the concept of a photon.

2.2 Radiation Particles

An incoming particles's energy is basically what defines its interaction with matter, as its energy increases, its velocity and momentum also increase, while its wavelength get smaller. There are three outcomes for each particle in an incident flux targetting a slab of matter:

Figure 2.1: Different outcomes for a particle interaction on a slab of matter.



Source: (Baumann and Kruckmeyer, 2019) [3].

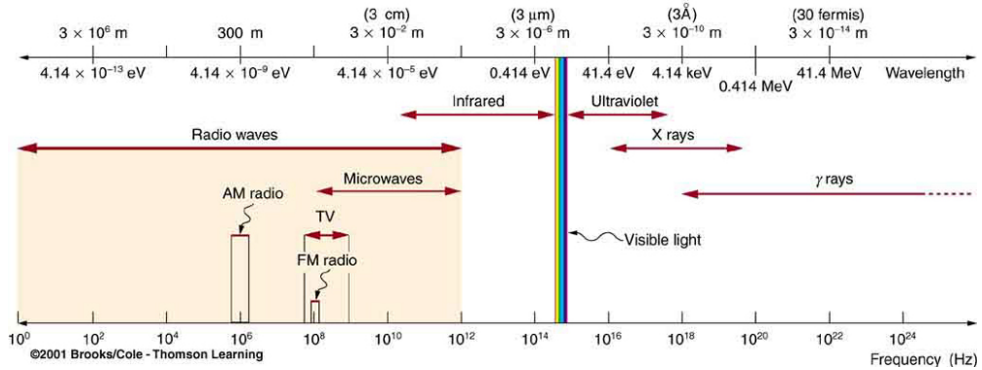
1. The particle will pass through the material without interaction, emerging from the other side with the same ingress direction and energy. (**Figure 2.1-a**)
2. The particle will interact with the material and emerge scattered and/or with its kinetic energy reduced. (**Figure 2.1-c-d-e**)
3. The particle will lose all its energy and be absorbed in the material. (**Figure 2.1-b-f**)

The main particles of radiation are: photons, ions, electrons, and nucleons (neutrons and protons).

2.2.1 Photons

Photons are the fundamental carriers of electromagnetic energy, they have no mass or charge and their energy determines the electromagnetic spectrum.

Figure 2.2: The electromagnetic spectrum, categorized by the photon energy in eV, as well as wavelength and frequency.

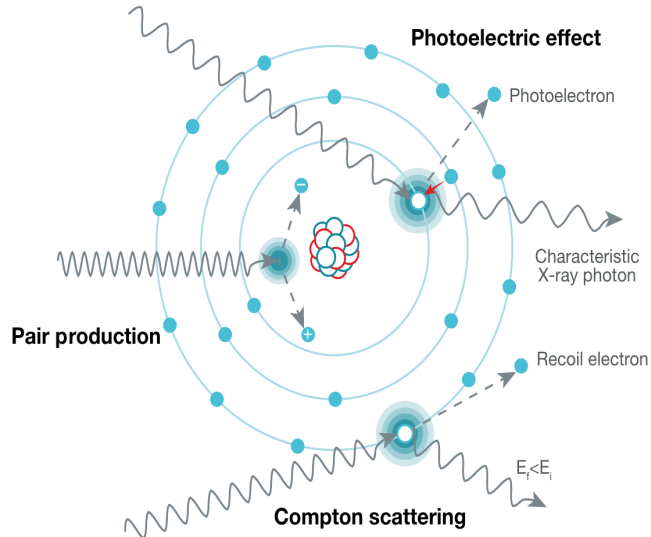


Source: (Urone and Hinrichs, 2020) [5].

The photon's lack of charge eliminates many interaction with other particles, since there is no Coulombic forces of repulsion or attraction. There are three main energy transfer processes between a photon and matter:

- **The Photoelectric Effect:** If the incident photon has sufficient energy to free an electron from the valence band, the photon is destroyed and all its energy absorbed, creating a photoelectron that leaves an empty space or a hole behind. At higher photon energies, the photon can excite an inner band electron, releasing a photoelectron and producing a X-ray photon as secondary reaction when an outer-shell electron fills the new vacancy created from the first absorption event. In cases when the photon energy is insufficient to create an electron-hole pair, the particle will traverse the material with no interaction.
- **The Compton Effect:** At intermediate energies, the photon loses some of its energy in a collision with a single electron, producing a free recoil electron and a scattered photon with lower frequency.
- **Pair Production:** At higher energies, an electron-positron pair is created as a gamma-ray photon passes near a nucleus in the medium. For a pair production to occur, the photon must have at least the rest energy of the two particles created, which is twice the rest energy of an electron (R. A. Serway and Moyer, 2005) [6].

Figure 2.3: The three main energy transfer processes of a photon with matter.



Source: (Baumann and Kruckmeyer, 2019) [3].

As a result of packaging, typically plastic, ceramic and metal, lower energy photons are usually not a concern. Higher energies, such as X-ray and Gamma-ray, can easily penetrate the package shielding and are the primary concern photons for microelectronics.

In terrestrial and space environments, X-ray and Gamma-ray fluxes are not significant compared to those from other radiation types, however it is commonly found in industrial and medical environments, where the charge production is dominated by the photoelectric effect.

2.2.2 Electrons

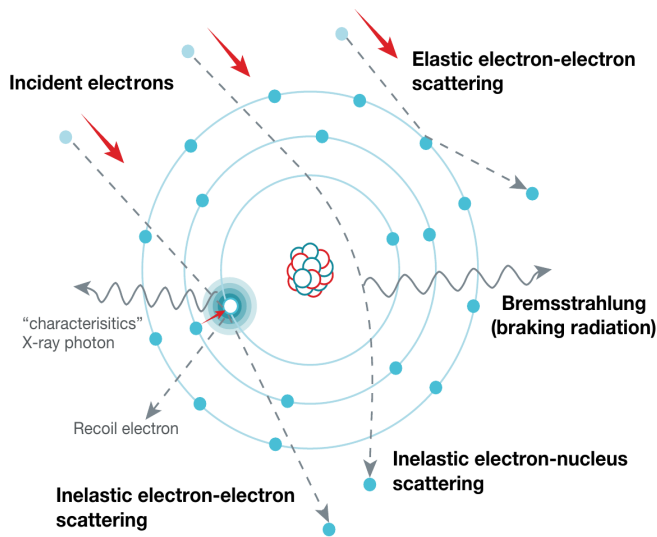
The electrons interact with matter via Coulomb forces. In the case of an electron-electron interaction, a repulsive force grows as the distance between them decreases. In elastic collisions, the incoming electron is deflected from its original trajectory or scattered. Considering an inelastic collision, the bound target electron absorbs some or all kinetic energy from the arriving electron and is promoted to a higher energy level.

In a similar way as the photon interaction described earlier, when an inner electron is excited and leaves a vacancy, this open spot is immediately filled by another electron from an upper energy state, emitting a photon whose energy is the difference between the transitioned energy states. If the electron new energy state momentum is different, in the case of indirect band gap materials, another particle will be transmitted to the material lattice, a phonon; which translates to vibration or thermal energy.

Conversely, in an electron-nucleus interaction, an attractive force grows as the distance between the electron and nucleus shrinks. One primary inelastic interaction in this case results in the direct emission of a photon. As the electron is attracted to the nucleus, it is decelerated, and the lost kinetic energy is emitted in the form of a photon. This interaction receives the name of breaking radiation or Bremsstrahlung.

Moreover, electron-electron scattering effects are larger in higher atomic number atoms, since they have higher electron densities.

Figure 2.4: The three main energy transfer processes of an electron with matter.



Source: (Baumann and Kruckmeyer, 2019) [3].

In terrestrial environments, the electrons usually do not have enough energy to effect on the reliability of microelectronics. On the other hand, for space, industrial and medical applications they can penetrate the package and damage the system inside.

2.2.3 Neutrons

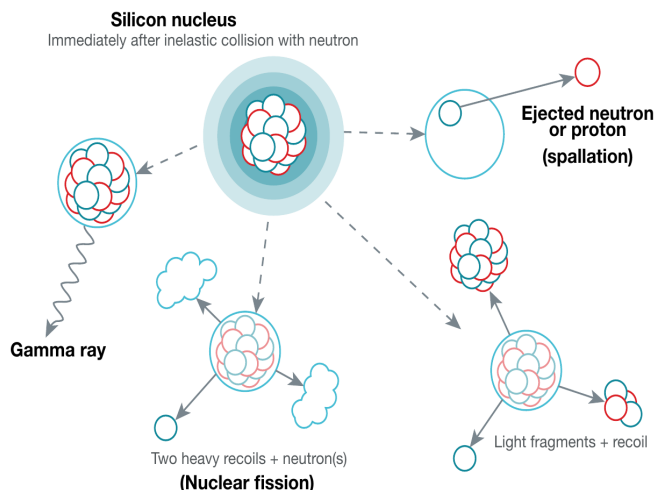
Neutrons do not have charge, as a result, Coulomb forces do not occur and they can not produce direct ionization as they travel through a material. Since their limited interactions, neutrons can cross an important thickness of matter without affecting it.

A neutron can experience elastic and inelastic nuclear reactions when colliding with a nucleus. For an elastic impact, the neutron transfers part of its kinetic energy to the nucleus, displacing it from its origin position. Each neutron-induced recoil nucleus is considered a heavy ion that causes direct ionization as it travels within the material.

When the neutron is absorbed by the material nucleus, an inelastic collision, the nucleus enters in a state of excitation and releases this excess energy with the emission of a secondary radiation, which depends on the nucleus type and the kinetic energy of the incident neutron. At a few tens of kiloelectron volts, the excess energy of the incident neutron is converted in the form of Gamma-ray photons. Increasing the kinetic energy of the irradiated neutron, from one to tens of megaelectron volts, the nucleus breaks apart into one or more light fragments (nucleons, light ions and Gamma-rays). This secondary radiation usually is responsible for the directly ionization of the material, and it is the dominant source of Single Event Effects on microelectronics, which will be seen in the following sections.

In certain types of elements, its nucleus will split into two nearly equal mass recoil fragments while emitting one or more neutrons. This interaction is called a nuclear fission, and is the basis of a nuclear reactor. In microelectronics, fission is not significant, since heavy compounds are found in impurity levels (parts per billion). For energy levels above 100 Mev, the incident neutron interacts with a single neutron or proton, ejecting it with a high kinetic energy. This reaction receives the name of spallation, and its secondary radiation will further interact with the material.

Figure 2.5: Inelastic neutron collision nuclear reactions.



Source: (Baumann and Kruckmeyer, 2019) [3].

Neutrons are one of the primary radiations in terrestrial environments, being the direct result from the interaction of cosmic-ray protons with the Earth's atmosphere. They are encountered from sea level to flight altitudes.

2.2.4 Protons

Protons have nearly the same mass as neutrons and they will interact the same way with matter in many cases. The main difference is that they will also interact via Coulombic forces, therefore directly ionizing materials. For kinetic energies below 50 Mev, Coulombic effects will dominate over nuclear reactions, protons will attract electrons and be repulsed by the nuclei of atoms.

Protons are the primary radiation found in space, and a significant amount will have enough energy to penetrate shielding and impact electronics.

2.2.5 Ions

Energetic ions are atoms that have lost some or all of their electrons, hence they are positively charged particles traveling at high velocities. Ions will affect the target atoms via electronic (direct ionization) or nuclear interactions (elastic and inelastic collisions).

Furthermore, heavier ions with more positive charge are more effective in generating charge over its trajectory. Heavy ions are the main cause of Single-Event Effects in space, although they are not a concern for terrestrial environments since they are rapidly absorbed by the atmosphere.

2.3 Radiation Environments

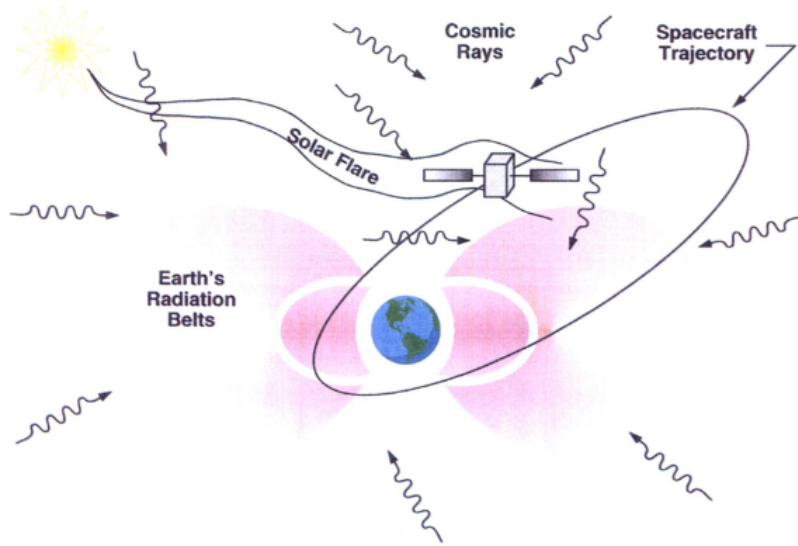
Radiation sources can be encountered in three primary environments: the space, where the natural radiation from the sun and other parts of the universe will directly influence in spacecrafts and artificial satellites functionality; the terrestrial environment (ground and atmosphere), in which most electronic systems operate; and specialized environments like medical, industrial and military sites, where man-made or artificial radiation plays an important role in numerous applications.

2.3.1 Space Environment

The space is probably the most "famous" environment for radiation. Outside the protective shielding of Earth's atmosphere, there are three radiation sources: Galactic Cosmic Rays (GCRS), predominantly comprising of protons from outside our solar system; Solar

radiation, consisting of low energy electrons and protons (Solar Wind) or energetic protons and heavy ions (Solar Flares) (Howard and Hardage, 1999) [7]; and finally, Radiation Belts formed by imprisoned energetic particles due to a planet's magnetic field.

Figure 2.6: Cartoon depicting the different radiation sources found in space: radiation belts, solar flares and galactic cosmic radiation.

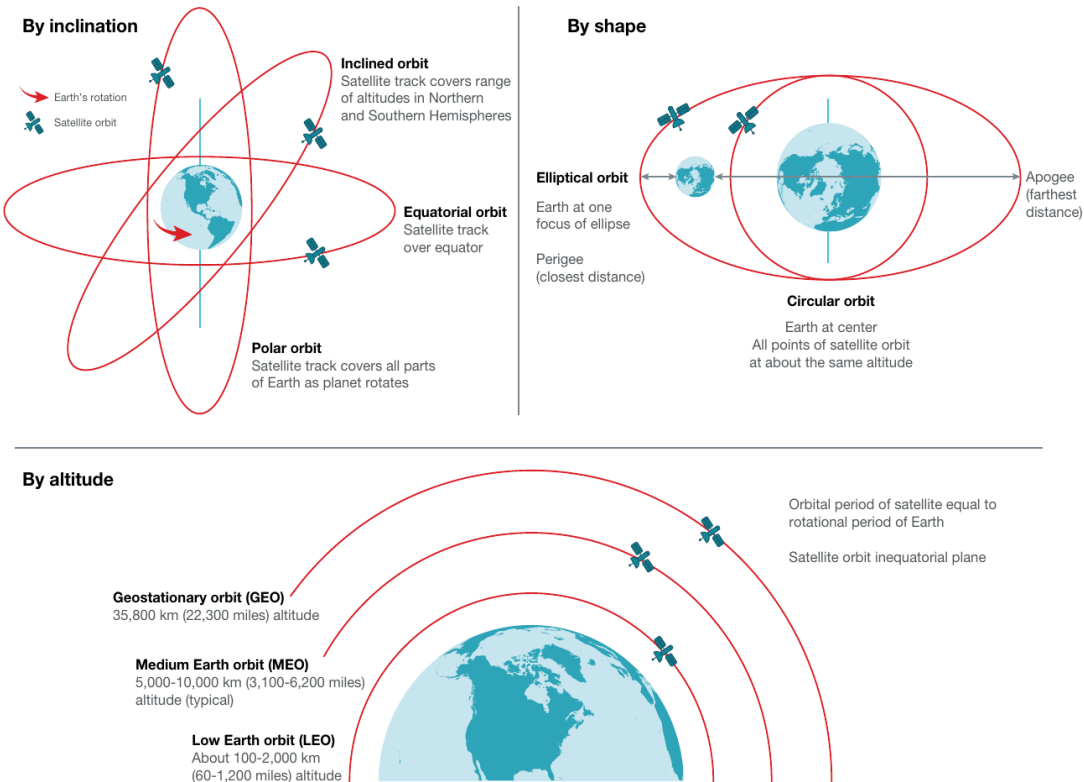


Source: (Howard and Hardage, 1999) [7].

Microelectronic components radiation exposure in space will be roughly a function related to the spacecraft orbit, mission duration and the amount of shielding protecting them.

The Earth's magnetic field has a varying effect according to the mission orbit. At higher altitudes orbits and/or orbits closer to the Earth's poles the protection is reduced, and more disruptive events can occur as a result of higher particle fluxes. Image 2.7 shows the different orbit types for a satellite.

Figure 2.7: Orbit types for a satellite based on altitude, inclination and shape.



Source: (Baumann and Kruckmeyer, 2019) [3].

As an example, a Geostationary orbit satellite operating during a period of 18 years will accumulate 100 Krad with a 5 mm aluminum shielding and only 10 Krad with a 10 mm shielding. At the same time, a satellite in Low Earth Orbit during 5 years and a 10 mm shield will absorb a dose of 300 Krad (Balen, 2010) [1].

2.3.1.1 Solar radiation

The sun is the greatest radiation source in the solar system, as it keeps converting hydrogen atoms into helium via nuclear fusion.

As commented earlier, radiation coming from the sun follows two mechanisms. The so called Solar Wind is a continuous flux of particles created by its super-heated atmosphere (corona). The temperature of the sun's corona is extremely high (\sim 1million K) that solar gravity cannot keep particles from escaping. This phenomenon is typically significant for externally mounted spacecraft components, and its effect is generally ignored when compared with other radiation sources (Howard and Hardage, 1999) [7].

Solar Flares occur around sunspots, regions of strong magnetic fields. These sunspots,

which appear as dark regions on the sun because they are a few thousand degrees cooler than their surroundings (Mukherjee, 2008) [2], present intense and unpredictable discontinuities in magnetic field strength that precipitate sudden bursts of magnetic energy and plasma stored in the corona. Also, the sunspots are related with the solar cycle, a period of 11 years characterized by approximately four years of reduced activity and seven years of increased activity. At the peak solar cycle, more sunspots appear on the sun and, consequently, more solar flares are created.

Another interesting fact is that solar radiation, while it can cause serious problems for space environment applications, also acts as protection for the terrestrial environment. The large number of particles creates an additional magnetic field around the Earth, shielding the planet from even higher-energy particles coming from the galaxy.

2.3.1.2 Galactic cosmic rays

Even the vast seemingly empty spaces between the stars are filled with matter and energy. Recalling a Parmenidean position: “You say there is the void; therefore the void is not nothing; therefore it is not the void”.

Galactic particles are believed to originate from supernova explosions, stellar flares and other cosmic interactions. GCR composition consists of about 85% of protons(ionized hydrogen), 14% of alpha particles(ionized helium) and 1% of heavier atomic nuclei (Balen, 2010) [1]. These particles typically have energies above 1 GeV, and the highest energy ever recorded excess 10^{20} eV.

The usual flux of these particles ranges close to 36000 particles/cm²-hour, compared to about 14 particles/cm²-hour that arrive the Earth’s surface (Mukherjee, 2008) [2]. As mentioned before, the solar activity cycle modulates the flux that hits the Earth’s atmosphere, dropping it during solar maximum when increased ionization deflects the incoming particles (Baumann and Kruckmeyer, 2019) [3].

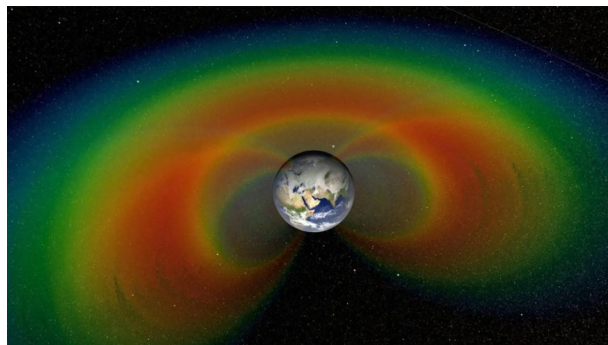
2.3.1.3 Radiation Belts

Radiation Belts are not primary sources in the sense that its radiation consists of captured particles from the sun and the galaxy. These belts are found around any planetary body with sufficient magnetic field energy to divert a particle trajectory. Besides Earth, Jupiter has an extremely powerful magnetic field being more than ten times that of Earth.

These trapped radiation regions around Earth are termed the “Van Allen Belts”, since they were discovered by Dr. James Van Allen and a team of scientists through a series of experiments starting with the first ever launched satellite by the United States, the Explorer I.

The Earth’s magnetosphere creates two permanent radiation belts. The inner belt, at the equator ranges from approximately 1.200 Km to 6.000 Km, contains high concentration of electrons of energies from 1 Mev to 5 Mev and protons of 10 Mev. The outer belt, ranging from the equator about 13.000 Km to 60.000 Km, is formed mainly by electrons with energies of 10 Mev to 100 Mev, and its particle population is highly sensitive to the solar activity (Baumann and Kruckmeyer, 2019) [3]. Seldom, a third belt can be observed, this transient radiation is related to the sun activity.

Figure 2.8: Cross-section cutaway of the Van Allen belts surrounding Earth. Blue and green represent lower fluxes, and orange and red correspond to high particle flux.



Source: (NASA, -) [8].

Another import characteristic related to the magnetosphere is the South Atlantic Anomaly(SAA). The Earth’s magnetic field axis does not point to geographic north and does not pass directly through the center of the Earth (Howard and Hardage, 1999) [7]. As a result, there is a deformation on the magnetic field that causes the inner belt to be lower over the South America off the coast of Brazil. Most of the radiation dose exposure that the International Space Station receives occurs while it flies through the SAA (Baumann and Kruckmeyer, 2019) [3].

While the particles present in the belts have lower energy when compared to Solar Flares and most GCRs, their concentrated flux levels can be dangerous if exposed for extended periods. Missions orbits and paths are programmed to minimize this exposure and, when possible, electronics are powered down during the time passing throughout the belts with the intention to reduce Total Ionizing Dose effects, which will be discussed later (Baumann and Kruckmeyer, 2019) [3].

2.3.2 Terrestrial Environment

Before 1978, radiation was considered to be a reliability issue for space applications, but not for electronics operating at sea level (Nicolaidis, 2011) [9]. The terrestrial environment can be viewed as the Earth's atmosphere from sea level to flight altitudes, typically up to a maximum of 22 Km. Two sources of radiation dominate in this environment: neutrons and alpha-particles. Since these particles event rates are low, Total ionizing dose and displacement damage are unusual; most failures are related to Single-event upsets, later explained in this chapter.

2.3.3 Alpha particles

In 1978, May and Woods from Intel introduced the first account of radiation-induced errors at sea level. They discovered that the Intel 2107-series ceramic package was contaminated with radioactive impurities from the water used in the fabrication process. The contamination was due to an old uranium mine present upstream along the river that the foundry had been built.

Radioactive impurities are found by trace amounts (small quantities that are often difficult to measure or detect) in materials used in the microelectronics manufacturing process. For an element to be stable, the ratio of neutrons and protons must be inside a certain range. Thus, an unstable nucleus will spontaneously decay emitting lighter particles until a stable ratio is reached. On these processes, the alpha particle (helium nucleus built with two neutrons and two protons as commented before) is the primary concern since it has the greatest ionizing capacity.

The predominant source of alpha particles in materials are the isotopes of uranium and thorium and their associated daughter products. The activity of a particular isotope is directly proportional to its abundance in nature and inversely related to its half-life (Baumann and Kruckmeyer, 2019) [3].

Furthermore, the alpha-particle emission energy is specific to the nucleus, and it is in a domain between 3 Mev and 9 Mev (Nicolaidis, 2011) [9]. In general, the majority alpha particles source is the package material (Mold compound, Flip-chip underfill and Eutectic Pb-based solder), not the materials used to create the semiconductor device (Processed wafer and metals).

When the industry realized the potentially risk of alpha particles for microelectronics in the early 1980s, material manufactures came up with a low-alpha specification of less than 0.01 alpha/cm²-hour. In the next decade, as new technologies scaled, the alpha particle sensitivity grew and a new standard was established of ultra-low-alpha (ULA) emission of less than 0.002 alpha/cm²-hour (Baumann and Kruckmeyer, 2019) [3].

Mitigation of alpha particles impact can be accomplished by using extremely high-purity materials, design rules separating sensitive parts of the circuits and through shielding the die from high emission materials.

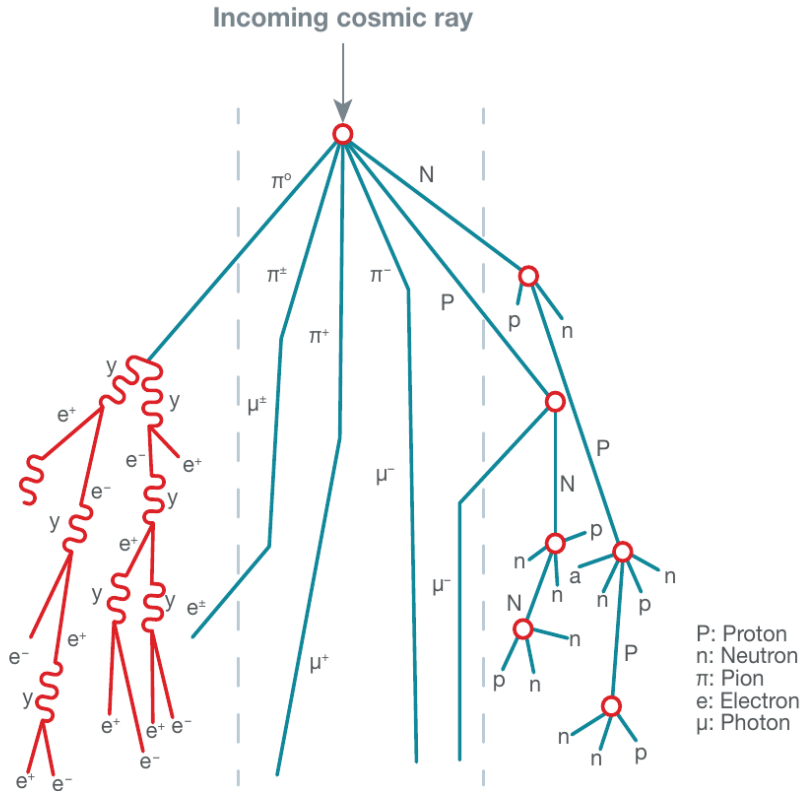
2.3.4 Neutrons

After May and Woods publication, Ziegler from IBM along with Landford of Yale University thought that cosmic radiation possibly had the same effect as alpha particles. Later, they found out that intergalactic particles with energies of more than 2 Gev can interact with the atmosphere and create secondary particles able to impact the semiconductor (Nicolaidis, 2011) [9].

Cosmic ray protons will undergo nuclear reactions with oxygen and nitrogen producing complex cascades of secondary particles such as: short-lived pions and kaons that decay into muons, neutrinos, gamma rays, electrons and positrons.

The actual flux that reaches sea level is only the sixth generation of particles, which corresponds in less than 1% of the primary flux (Mukherjee, 2008) [2]. This generation consists of neutrons, protons, electrons and muons and pions.

Figure 2.9: Particle shower created in the upper atmosphere by cosmic ray protons interaction with nitrogen or oxygen.



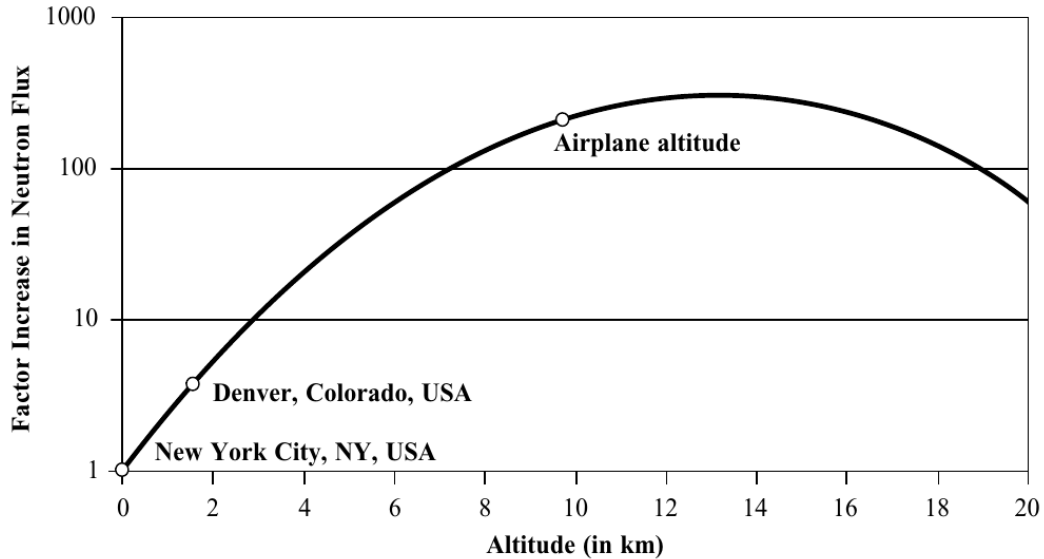
Source: (Baumann and Kruckmeyer, 2019) [3].

Pions and muons have a mean lifetime of nanoseconds and microseconds respectively, and protons and electrons will be effectively attenuated by Coulombic forces. Neutrons, on the other hand, have a mean lifetime of 10-11 minutes and no charge, so they survive longer.

The resulting neutron flux occupies a wide range of energies and is strongly related to the altitude and longitude. At flight altitudes, this flux can be hundreds of times higher than it is at sea level, as a result, it dominates reliability in avionics. As seen before, alpha particles can constitute a large portion of the failure rate in devices at sea level, however, at flight altitudes they become a negligible fraction since they are only dependable in intrinsic impurity levels of materials.

The neutron flux peaks and saturates at around 15 Km, also known as Pfotzer Maximum (Mukherjee, 2008) [2]. Figure 2.10 shows a rough approximation of how the flux varies with altitude.

Figure 2.10: Variation of neutron flux with altitude. Comparison between a high-elevation city and commercial flight altitude.



Source: (Mukherjee, 2008) [2].

Moreover, the neutron flux increases from equatorial to polar regions. There is a weak shielding in areas where the Earth's magnetic field approaches normal orientation.

Each location on Earth is associated to a quantitative value called Geomagnetic Rigidity (GR) defined as the minimum momentum necessary for a normally incident particle to overcome the Earth's magnetic field and reach the sea level (Mukherjee, 2008) [2]. Hence, higher the rigidity of a site, lower is the terrestrial cosmic ray flux. Typically, the latitude can modulate the neutron flux by a factor of 2x at sea level and approximately 5x at flight altitudes (Baumann and Kruckmeyer, 2019) [3].

In 1995, Baumann from Texas Instruments showed another important aspect about neutrons. The boron compound, used extensively in semiconductor production, is highly unstable when exposed to thermal neutrons (lower energy neutrons around 0.03 eV). Two isotopes of boron exist: boron-10(19.9% abundance) and boron-11(80.1% abundance). Unlike most isotopes that emit gamma photons, the boron-10 nucleus breaks apart after absorbing a thermal neutron and releases a Lithium-7 recoil nucleus and an alpha particle; both of these particles can generate charges in silicon and cause SEEs.

The cosmic-ray neutron flux cannot be easily reduced at the integrated circuit level. Neutron shielding schemes only partially work with lower atomic number or hydrogen-rich materials as concrete, which are not suitable for the majority of applications like portable

electronics for example. Conversely, there are several ways to reduce the thermal neutron interaction with the boron-10 isotope; the most straightforward approach is to simply eliminate and use only boron-11.

2.3.5 Specialized Environment

Specialized environments are related to specific applications where man-made artificial radiation is found; it can be categorized into medical, industrial and military.

Figure 2.11: Examples of specialized radiation environments.



(a) Two nuclear reactors at the TVA Watts Bar Nuclear Power Plant located in Tennessee.



(b) Aircraft carrier USS Carl Vinson, powered by two nuclear reactors, docked near San Diego, CA.



(c) X-ray machine.

Source: United States Environmental Protection Agency (EPA).

2.3.6 Medical field

In the medical field, radiation exposure normally happens in diagnostic and treatment machines as X-ray or proton-beam. Electron-beam and gamma-rays are also used for sterilizing

surgical instruments and implantable electronics. TID effects, which will be seen in the next sections, are the main concern for electronics in a medical environment.

Implanted microelectronics in a patient, like pacemakers and cardio defibrillators, are unlikely to be exposed to any radiation that would damage them, since humans are much more sensible to it if compared to silicon devices. Furthermore, considering the fact that the majority of the radiation equipment is used over long periods of time on many patients, internal electronics can accumulate high TIDs; metal shielding is commonly used in these machines as a counter measure.

Conversely, image sensors will necessarily be exposed to X-rays, accumulating radiation, and must be periodically replaced. Because this accumulated dose will shift the device parameters, self-test startup routines can be performed to detect and alert the user when the machine needs maintenance.

2.3.7 Industrial field

The use of radiation in industry is extensive. For example: in the processing of materials, in sterilization, in inspection and monitoring of physical material properties, in the defect inspection of components and in security screening applications. Radiation sources can be divided into sealed radioactive materials that continuously emit radiation and machines that produce radiation by accelerating particles; the charged particles are accelerated using high voltages and can act directly as a source or be directed onto a target material converting the incident radiation into secondary radiation.

Microelectronics in areas where operators are present are usually not at risk, for radiation sources must be well-shielded and controlled to levels deemed safe for the human body. Although, there are areas where electronics cannot be shielded such as in imagers, dosimeters, nuclear power plants with gauges, liquid-level and other detectors; therefore, specially designed radiation-hardened devices are necessary.

Nuclear power plants are going to be fundamental energy sources in the future, considering the surge in energy consumption since the boom of artificial intelligence and electronic vehicles.

Finally, TID effects are the primary concern in industry, and the radiation commonly found are X-ray, gamma-ray, e-beam and neutrons.

2.3.8 Military field

The military field, often regarded as Defense field, can be thought as a mixture of the industrial and medical fields with high-standard electronic devices. In addition to nuclear reactors installed in some navy vessels and submarines, the detonation of nuclear weapons will produce radiation. The gamma-ray and neutron emitted by a nuclear detonation and the subsequent Electromagnetic Pulse (EMP) are the primary concern for microelectronics outside the blast zone.

2.4 Radiation Effects

The radiation effects on microelectronics can be separated into three fundamental groups:

- **Single-event effects (SEEs):** are random and instantaneous disruptions activated by the passage of single particles.
- **Dose effects:** are long-lasting parametric shifts due to charge accumulation over a period of time. Dose effects can be further divided in **Total Ionizing Dose (TID)** and **Displacement Damage (DD)**.
- **Dose-rate effects:** are similar to SEEs effects, although they are induced by an extremely high dose rate over a brief time interval.

In conductor and semiconductor materials, any excess charge generated by an incident ionizing particle will be quickly dissipated by the drift and diffusion currents or compensated with the recombination of electron-holes. This momentary charge burst can only produce SEEs errors, because no charge is stored.

Evaluating now insulating materials, the consequences of a striking particle are completely different. Insulators are known for having wide band gaps, low free-carrier densities and low carrier mobility (at least for holes) (Baumann and Kruckmeyer, 2019) [3].

Before proceeding to the next sections, it is important to understand two fundamental concepts used to describe radiation effects: Linear Energy Transfer and Cross-Section.

Linear Energy Transfer (LET) is a measure of energy deposited per unit length, typically reported in units of megaelectron volts-square centimeters per milligram. It describes

the average energy loss by a particle per unit length of a traversed material (Nicolaidis, 2011) [9], or the amount of energy that a particle transfers to a medium per unit distance traveled.

Cross-Section is a measure of the probability that a specific interaction will occur when particles traverse a target material (Baumann and Kruckmeyer, 2019) [3]. It defines the effective area of a specific material nucleus for interaction with a particle, being reported in units of barns/particle, where one barn equals $10^{-28} m^2 = 10^{-24} cm^2$.

For example, in silicon, the total neutron cross-section decreases from 1.95 barn at 40 MeV to 0.6 barn at 200 MeV (Nicolaidis, 2011) [9]. The cross-section can be calculated by the following equation:

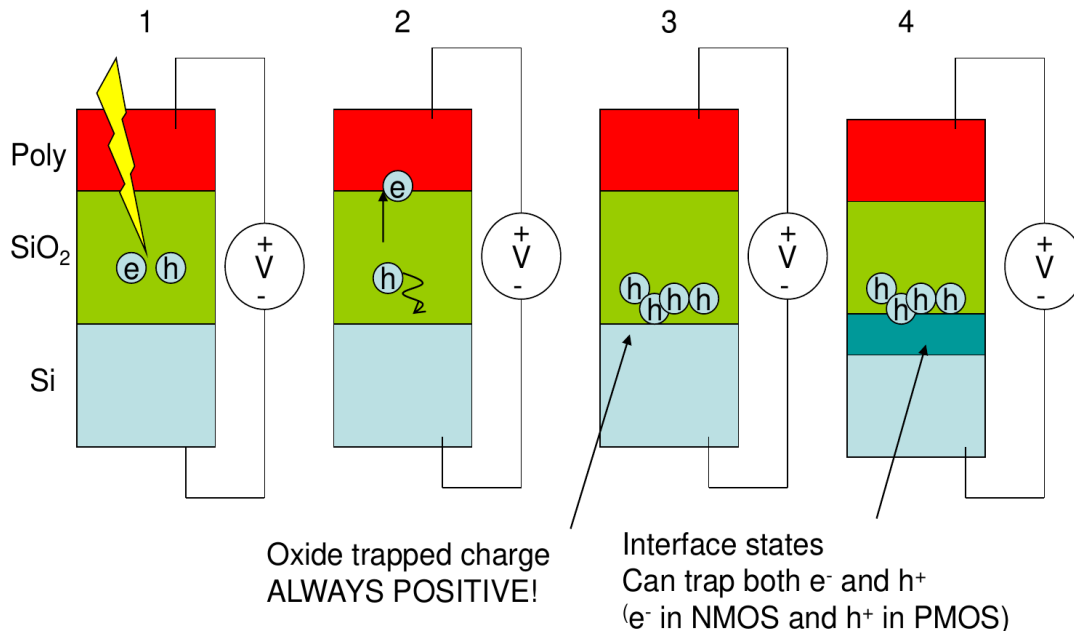
$$\sigma = \frac{N}{F \cdot \cos\Phi} \quad (1)$$

Where N represents the number of observed errors, F is the total particle fluence given in particles/cm² and Φ is the particle beam incident angle. The particle fluence can be obtained by integrating a particle flux over time (Balen, 2010) [1].

2.4.1 Total Ionizing Dose

Considering a MOS device, the key mechanism driving TID is the generation, transport and trapping of holes in the metal-oxide material used in the gate (Silicon Dioxide).

Figure 2.12: The process responsible for the Total Ionizing Dose effect in a MOS device.



Source: Semiconductor Devices Class slides (Gilson Wirth, 2024).

Figure 2.12 describes the process behind the charge accumulation in the silicon oxide layer; the final result resembles an “unwanted programmable memory” (Flash), where the different floating gates will store charge and modify the transistor drain current characteristic curve.

The first step represented in the image (1), already discussed in the previous sections, is the formation of electron-hole pairs when an incident radiation particle energy is absorbed. If the oxide used were an ideal material and charges were truly immobile, all the electron-hole pairs would recombine and the following steps in Figure 2.12 would not exist, as well as TID. Although, electron mobility is much higher than that of holes in oxides; consequently, the second step (2) illustrates the transport of an electron by diffusion and, in this case where there is an electric field, a drift current.

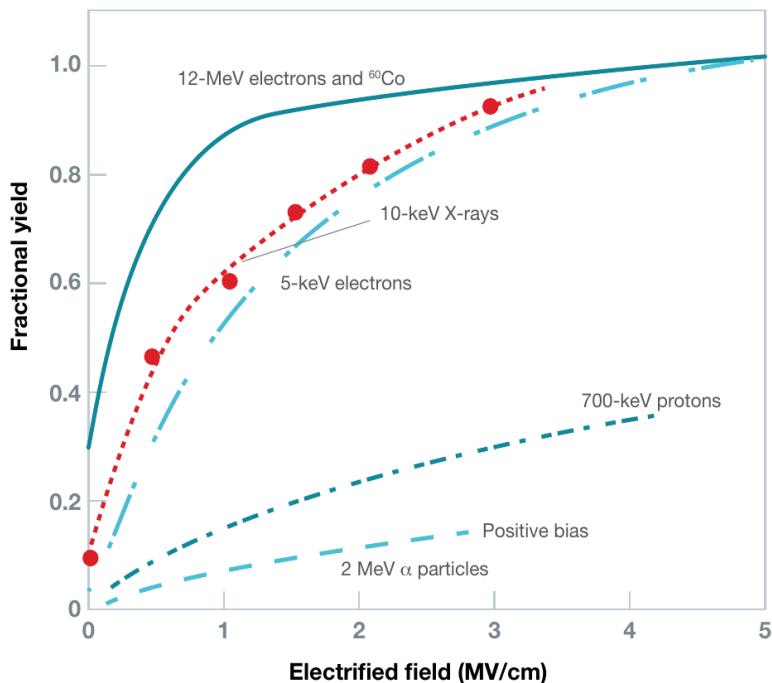
This is the reason why satellites are usually powered down when passing through radiation belts, as commented before. The presence of a strong electric field increases the chances for an electron to escape.

After the electron-hole separation, the hole itself starts migrating to the oxide/channel interface. This process breaks chemical bonds and releases trapped protons (hydrogen ions), which follow the same direction as the holes. During this journey, part of the holes are caught in mid-band-gap traps, initially causing a positive charge buildup, (3) in Figure 2.12; the other

part is captured at the interface, where they create positive, negative or neutral states, (4) in Figure 2.12. These interface traps are a direct result from the hydrogen ions released (Balen, 2010) [1], or are naturally created by defects on the oxide that forms oxygen vacancies.

TID is evaluated as the energy absorbed by a unit mass of material when exposed to ionizing radiation, and it is measured in units of rad (radiation-absorbed dose). Moreover, the fraction of not recombined holes in the gate oxide receives the name of “fraction yield”, and it can be plotted as a function of the present electric field and the radiation type as showed in the Figure 2.13 below.

Figure 2.13: Fractional Yield x Electric Field for different radiation types.



Source: (Baumann and Kruckmeyer, 2019) [3]

As it can be seen, the most effective radiation is X-rays, followed by electrons. Even though ions have a greater LET, fractional yield is inversely proportional to the charge density generated within the oxide volume; it may be a little counter-intuitive, but the electron-hole recombination rate is a strong function of the amount of excess charge in the vicinity.

The predominant failure in commercial MOS devices is due to the increased leakage current induced by the positive charge trapped in the isolation oxide. Other consequences of TID, also related to accumulated charges inside the oxide and near the interface, are connected to parametric shifts: the threshold voltage decreases, the carriers' mobility are modified, and

the intrinsic characteristic noise is increased (Balen, 2010) [1].

Tunneling and thermalized electrons from the silicon are able to neutralize the trapped holes, permanently removing the charge. To speed up this process, the device can be heated to temperatures around 100 °C; a strategy known as annealing.

Ultimately, new technologies are more resilient for TID effects. The reason is related to better gate oxide materials and deposition techniques; also, less volume of it is used as the transistor is scaled down.

2.4.2 Displacement Damage

Displacement Damage (DD) is another type of dose effect. It is connected to the accumulation of physical damage to a crystal structure due to neutron and proton radiation doses, resulting in the degradation of the material's electrical properties.

Radiation-induced DD effects are referred to as nonionizing energy loss (NIEL) mechanisms. Unlike TID, which is the surface accumulation of trapped charge and interface states, DD is a volumetric effect that leads to the formation of traps throughout the bulk of active device regions.

At sufficiently high absorbed doses, DD causes mobility degradation and free-carrier reduction; eventually heading to a decrease in the device's drive strength and switching speed.

2.4.3 Single Event Effects

One famous example of how SEEs may impact microelectronics happened in 1999, with the high-end server line from Sun called "Enterprise". At that time, the Enterprise was Sun's flagship (most important product), with a price ranged from \$50,000 to more than \$1 million and was used by major companies such as America Online and Ebay.

During that year, some customers reported occasionally crashes for apparent no reason, and one company declared that their server had crashed and rebooted four times within a few months (Nicolaidis, 2011) [9]. One statement by a customer, criticizing the product, explains how bad Sun's brand image was damaged: "It's ridiculous. I've got a \$300,000 server that doesn't work. The thing should be bulletproof!".

After months of investigation, Sun identified that soft errors in the cache memory were the root problem. To solve this situation, the memories in the server were replaced by redundant

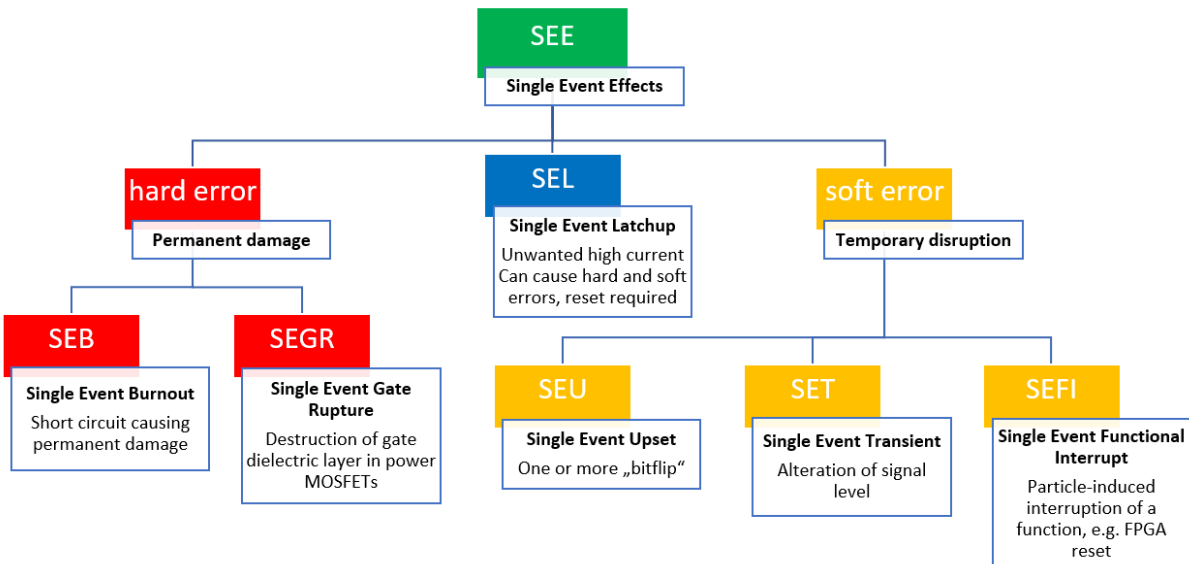
or mirrored caches, meaning that if the first cache fails, the second one is a back up. Sun reported that the issue had cost huge amount of human hours and tens of millions of dollars.

Single-event effect is defined as any measurable or observable change in a device's state or performance due to an energetic particle strike (Nicolaidis, 2011) [9]. Soft errors are a subset of SEEs, they are events in which only data is corrupted, the device itself still continues to work. In contrast, hard errors are permanent hardware failures.

When SEEs occur in combinational logic or analog circuits with no memory, the disruption is transient and self-recovering; no external input is required to restore the system state. However, in digital sequential or memory components, and in analog systems as sample-and-hold circuits, the sudden charge burst generated by radiation can modify the state of the impacted node; in this situation, until a subsequent write operation that will clear the wrong information is issued, the data state read cannot be trusted. Furthermore, the physical effects of a destructive SEE will be the same as those observed in nondestructive, with the crucial exception that the device is permanently destroyed.

SEEs are divided into many subcategories, and their definitions and classifications may vary across different works and over time; for this thesis, Figure 2.14 summarizes them.

Figure 2.14: Single Event Effects classification diagram.

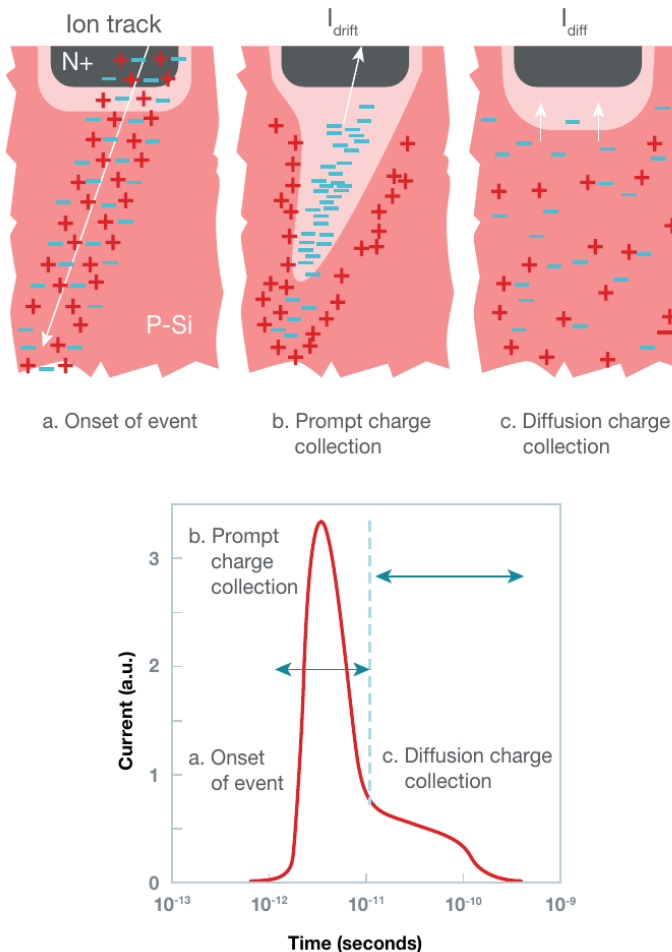


Source: (Horn, 2021) [10]

Every ion that reaches the silicon device active region will create an ionization path and potentially cause a SEE, it all depends on the ion LET, trajectory, energy, and other numerous

details about the circuit design. Figure 2.15 illustrates the basic mechanism responsible for a SEE when an ion strikes a reversed-biased junction, the most-sensitive part of microelectronics (Baumann and Kruckmeyer, 2019) [3].

Figure 2.15: Phases of charge collection and resulting transient current caused by the passage of a high energy ion.



Source: (Baumann and Kruckmeyer, 2019) [3]

Along the traversed path, the particle leaves a high density excess of electron-hole pairs behind. Two processes address this non-equilibrium situation: **charge recombination and charge collection**. As commented before in the TID section, if the carriers were completely immobile, all electron-hole pairs would recombine and quickly eliminate the excess charge; although, this scenario does not happen in real materials.

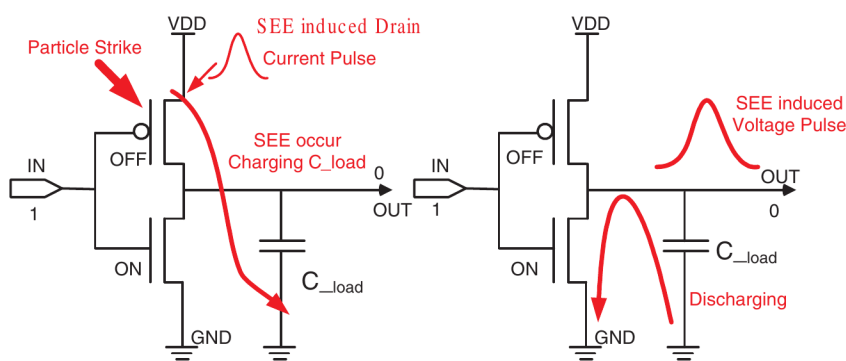
Part of the charge carriers will be transported by diffusion and drift currents and will be collected by the circuit node(or junction) capacitance. If the resulting ionization track crosses or comes close to the depletion region, the electric field will effectively separate electron-hole

pairs before they recombine, maximizing the charge collection; this condition is called “Prompt charge collection”, (b) in Figure 2.15, and it is the direct consequence of the drift current (I_{drift}). The prompt collection phase lasts a few nanoseconds and is followed by a slower charge-collection phase, dominated by the diffusion current (I_{diff}), (c) in Figure 2.15. The overall result is the creation of a short period current pulse with a duration ranging from hundreds of picoseconds to tens of nanoseconds (Balen, 2010) [1].

The charge collected (Q_{coll}) is a function of the ionizing particle’s energy and trajectory, silicon substrate and doping and the local electric field (Wang and Agrawal, 2008) [11]. If enough charge is collected, or if the charge injected by the current pulse at a sensitive node exceeds the node critical charge (Q_{critic}), a voltage pulse will be induced or the junction state will be modified. The most sensitive or critical nodes in CMOS circuits are the PN junctions from the “off” transistors.

Furthermore, the critical charge at a given node can be approximated by the product of the node’s capacitance with the power supply voltage: $Q_{critic} = C_i \times V_{dd}$ (Nicolaidis, 2011) [9]. Typical values for the critical charge are around 1-2 fC in SRAM devices and 20-30 fC in DRAM technologies. Figure 2.16 shows how a voltage pulse is created when the drain terminal of a PMOS device is hit in an inverter circuit. The initially “off” transistor will become momentarily conductive, as the drain-well terminal is “short-circuited” across the depletion zone. The parasitic capacitance at the output circuit will be charged along the induced current pulse duration and discharged when the charge equilibrium is reestablished.

Figure 2.16: SEE-induced current pulse at a CMOS inverter translated into a voltage pulse.



Source: (Wang and Agrawal, 2008) [11]

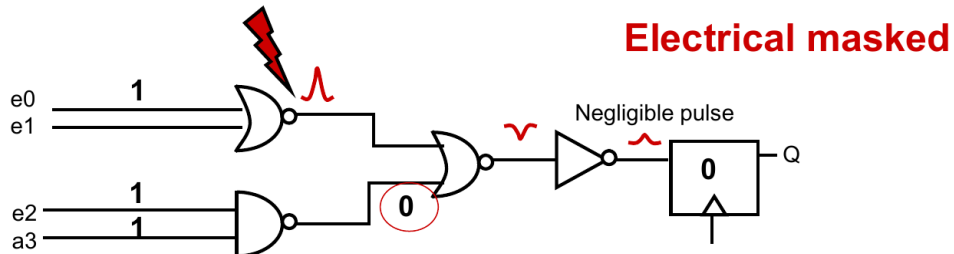
All subcategories depicted in Figure 2.14 are generated by the same process described, albeit they differ in the follow-up consequences to the affected circuit.

A **Single Event Transient (SET)** is defined as a momentary voltage or current spike at a node of a circuit. In digital combinational circuits, this transient can propagate through subsequent gates and eventually cause an “indirect” Single Event Upset (SEU) if it is captured by a memory element. In analog circuits, this transient may propagate to an output pin, disturbing amplifiers and comparators; also, for mixed circuits, it can generate erroneous voltage levels on sampling capacitors when they are in hold mode. A SET is often referred as an archetypal event from which all SEEs are ultimately derived, it will either manifest only as an SET or be mapped into one of the other several different types of SEE responses (Baumann and Kruckmeyer, 2019) [3].

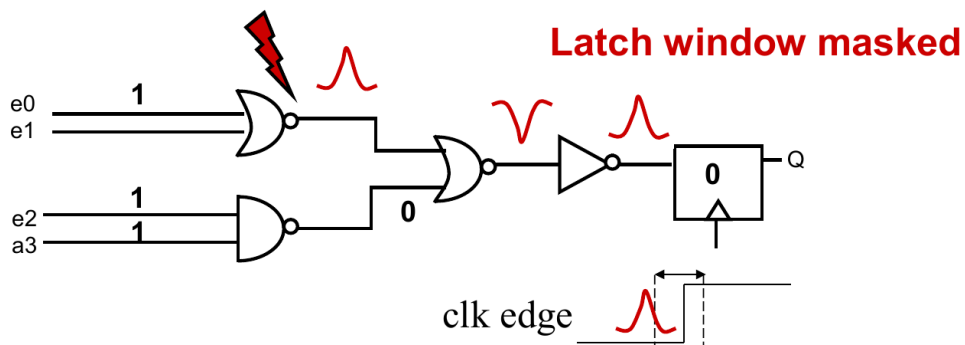
There are several obstacles a SET needs to overcome in a digital circuit before being translated as a SEU. In electrical masking, the original pulse amplitude will be attenuated by different logic gates, arriving at the memory cell as a small disturbance that is not captured by the element digital threshold voltage. In logical masking, there is no valid path for the incorrect input; therefore it will not be transmitted by the logical port.

For latch window masking, the erroneous pulse occurs outside the clock capture window (rising edge or falling edge). The probability that a SET will be captured in sequential components increases linearly with the circuit clock frequency (Baumann and Kruckmeyer, 2019) [3]. Figure 2.17 exemplifies the described masking mechanisms.

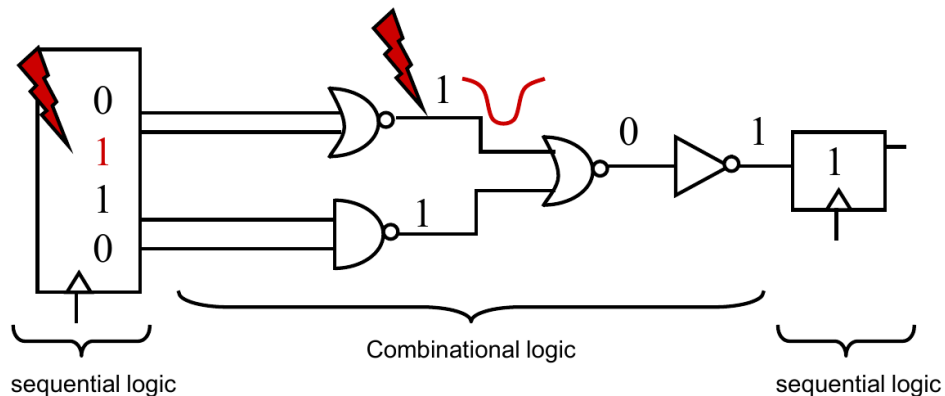
Figure 2.17: Examples of different masking types in combinational logic circuits.



(a) Electrical masking.



(b) Latch window masking.



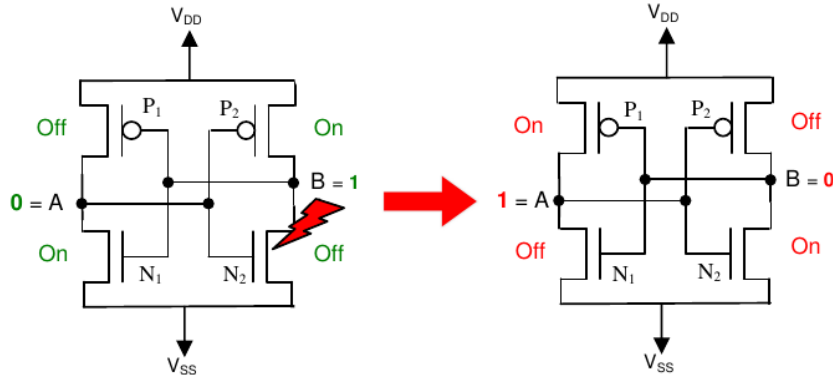
(c) Logic masking.

Source: Semiconductor Devices Class slides (Gilson Wirth and Fernanda Kastensmidt, 2024).

A **Single Event Upset (SEU)** causes a persistent error and it is defined as the change in state of a digital storage component such as a bit of a DRAM or SRAM, a latch or a flip-flop. Figure 2.18 describes a similar situation to the one before, with a single inverter (Figure 2.16); it represents what happens to a memory cell that uses cross-coupled inverters, or positive feedback, to store the data state when a particle strikes a sensitive node. In this example, the originally inactive NMOS device (N_2) is forced to conduct when an ion hits the PN junction of the drain terminal; the high state of node B turns to low, and at the same time,

the opposite occurs with node A.

Figure 2.18: SEE-induced bit-flip in a memory element.



Source: (Balen, 2010) [1]

A SEU flipping the data state in a single memory bit is known as a single-bit upset (SBU), whereas a large event that flips several bits from the same data word is called as a multiple-bit upset (MBU).

A Single Event Functional Interrupt (SEFI) is a type of SEE that can occur in digital devices, and it is a direct consequence of a critical bit-flip (SEU), which means that an important register controlling system operations and routines is suddenly changed. A SEFI may erroneously initiate a built-in test sequence, trigger a system reset, cause the device to lose part of its functionality and execute incorrectly or creates a system interruption. Most SEFIs require a level of external intervention, usually a reset or power-down reset to restore the system.

A Single Event Latchup (SEL) is a potentially catastrophic state lead by an unintended low-resistance path between power and ground, which remains after the triggering event dissipates. The high-current condition is maintained until the component is permanently damaged or the circuit power is interrupted. Latchup is a well-known reliability concern for CMOS and BiCMOS bulk technologies.

A Single Event Burnout (SEB) is classified as a hard error, which means it causes permanent damage to the device. A SEB is associated to power devices and is a consequence of an induced localized high current or voltage that creates thermal damage or “burns out” the device.

A Single Event Gate Rupture (SEGR) also results in irreversible damage to the device, therefore, it is a hard error. It is related to the gate dielectric rupture, allowing current to flow and changing the circuit characteristics. Due to high currents and voltages in power

devices, SEGRs are more common in power transistors (Balen, 2010) [1].

Unlike TID, new technologies are more vulnerable to Single Event Effects. Lower capacitances and supply voltages yields to lower critical charge (Q_{critc}), meaning that less energetic particles are able to create SEEs. The increase in the circuit density, complexity and frequency are also important factors that make modern devices more sensitive to these radiation effects.

2.4.4 Dose Rate Effects

Dose rate effects, also called prompt dose events, can be similar to SEEs, though differ since the whole device is irradiated at once. This type of effect is induced by the detonation of a nuclear weapon, which generates intense pulse of gamma radiation, X-rays and neutrons; the high flux of ionizing radiation produces photocurrents in the device's junctions that can temporarily disable the functionality of the device or produce a permanent damage triggered by SEL, SEB or SEGR.

2.5 Radiation Effects Mitigation

Radiation effects mitigation can be classified into prevention and recovery. Prevention techniques are related to adapting the fabrication process or the project layout. Materials purification and shielding are the most straightforward methods, however they may not be sufficient in many cases.

Purification processes cannot completely eliminate all material impurities and, although physical shielding can be very effective, it is not suitable for many applications. The costs of space-related missions are strongly related to the mass of a satellite or spaceship, as well as in aviation.

Other approaches may target the reduction of the collected charge (Q_{coll}) by using additional well isolation (triple-well or guard-ring) or replacing the bulk silicon well-isolation with silicon-on-insulator (SOI) substrate material (Wang and Agrawal, 2008) [11].

Recovery techniques can be achieved either via software or hardware. Software methods are less expensive and present great alternatives for the use of COTS devices in critical applications, although they are less efficient. Hardware methods are more expensive, can consume more of a device's area and demand more power. However, when implementation

is possible, they offer better performance.

Redundant designs as triple modular redundancy (TMR) with a majority voter are widely used (Wang and Agrawal, 2008) [11]. With spacial redundancy, the same hardware is replicated N times, where N is the number of input voters; considering a temporal redundancy, the hardware will perform the same function N times, each time spaced by a time period. Another method of recovery is Error Detection and Correcting (EDAC), commonly used in memories and communication systems. These memories will store parity bits to a group of data bits to make the number of 1s either even or odd for example, or use some data codification technique as Hamming Code. A checksum is also considered an error detection method, and was implemented to the PSoC 6 system communication channel.

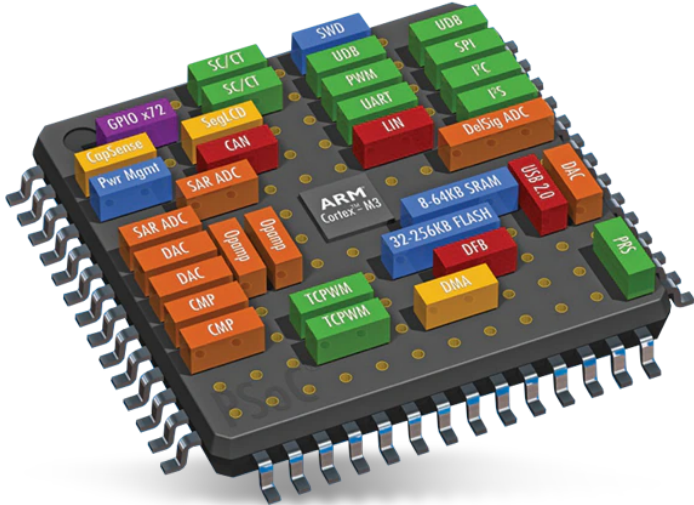
Another mitigation technique that can be seen as either preventive and recovery is scrubbing, which is the periodic re-writing of configurations. Scrubbing is usually related to FPGA systems, where the SRAM configuration registers are constantly overwritten with the same information.

Devices that present one or more of these mitigation techniques are often called radiation-hardened devices, which are electronic components designed to withstand and reliably operate in radiation environments or critical missions. Furthermore, the number of chips used in aerospace applications is usually small to accommodate specific modifications on all chips, therefore a mixture of radiation-hardened ASICs and COTSS chips are adopted.

3 Programmable System on Chip

This chapter provides the basics of a Programmable System on Chip (PSoC), presenting the device later used for the proposed monitoring system, the PSoC 6. It describes the most important characteristics from the device and its peripherals, paving the way to understand the reason for some design choices made in the monitoring system.

Figure 3.1: Programmable system on chip example



Source: (Mouser Electronics, 2025)

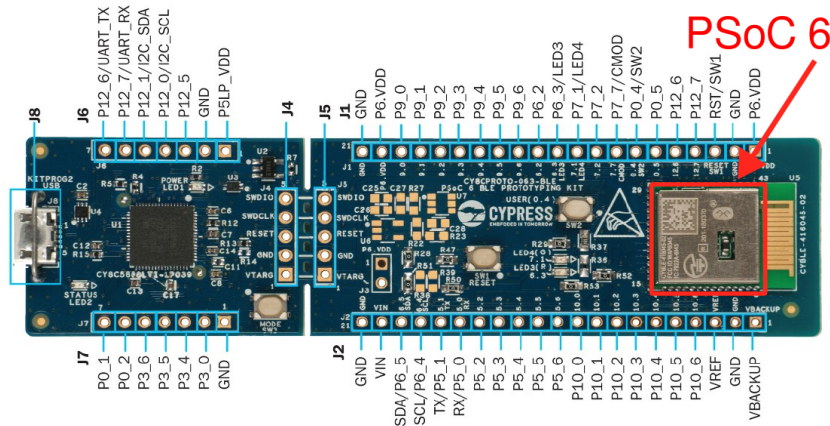
A programmable system on chip is a family of integrated circuits from Cypress (now Infineon). A PSoC can be described as an IC that combines a microcontroller unit (MCU), memory, and analog and digital blocks with a programmable routing network (Figure 3.1). It offers flexibility for the creation and prototyping of numerous embedded applications without requiring external components.

The main difference between a System on Chip (SoC), present in today's smartphones (e.g., Snapdragon, Apple A-series), many IoT devices and automotive systems, and a Programmable System on Chip is the level of programmability, as the name suggests, and the degree of integration of the analog and digital blocks. Therefore, they are usually targeted for different purposes and applications.

3.1 PSoC 6

The evaluated PSoC in this work is the PSoC 6, which is part of a development kit from Cypress (Figure 3.2). The PSOC 6 family is designed as a ultra-low-power architecture on a 40 nm process node, targeting IoT applications; the device used in this work has a Bluetooth Low Energy module and dual-core 150-MHz Arm Cortex-M4 and 100-MHz Arm Cortex-M0+ processors as its main distinction features (Infineon, -) [12].

Figure 3.2: PSoC 6 mounted in the development kit Infineon CY8CPROTO-063-BLE



Source: (Infineon, -) [13].

All features from the PSoC 6 are illustrated in Figure 3.6, and some of its main components used for the error identification system are summarized below:

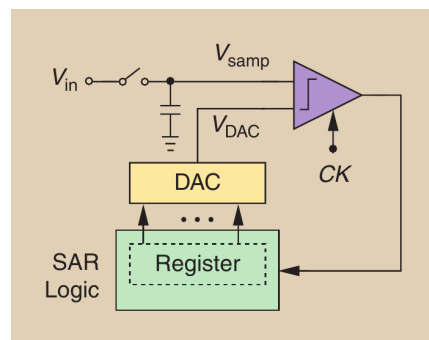
1. Dual-core 32-bit ARM processors (150-MHz Cortex-M4 and 100-MHz Cortex-M0+);
2. One Successive Approximation Register (SAR) 12-bit, 1-MspS ADC;
3. One 12-bit, 500 kspS continuous-time DAC;
4. Two DMA controllers with 16 channels each;
5. Eight Serial Communication Blocks (SCBs) configurable as SPI, I²C or UART;
6. Thirty-two timer/counter/pulse-width modulators (TCPWMs).

3.1.1 Analog to Digital Converter

There are several types of ADC architectures, e.g., Flash, SAR, Sigma-Delta, each of which involves different trade-offs between speed, power consumption, accuracy and area. The SAR design, present in the PSoC 6, consists of a comparator, a state machine and a DAC (Figure 3.3), hence achieving power and area savings at the expense of speed.

This topology performs a recursively binary search until the DAC output converges to the analog input, taking N clock cycles to resolve N bits.

Figure 3.3: Basic SAR architecture



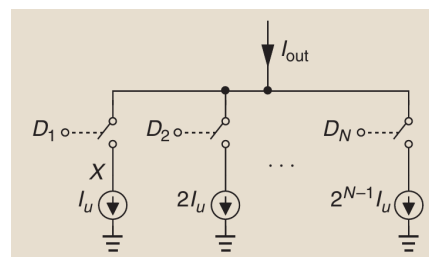
Source: (Razavi, 2015) [14].

3.1.2 Digital to Analog Converter

The PSoC 6 DAC architecture is not directly disclosed to the public, however, due to the converter specifications, it can be inferred that a Current-steering, a Current-switching, or a capacitor DAC design is used.

Image 3.4 shows a current-switching DAC example, where each input bit controls a weighted current source.

Figure 3.4: Simple binary-weighted current-switching DAC



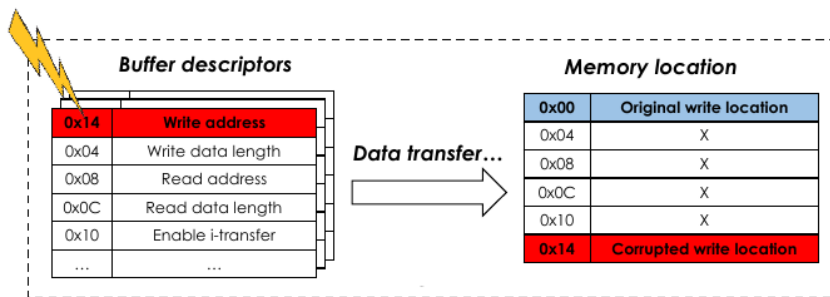
Source: (Razavi, 2018) [15].

3.1.3 Direct Memory Access

A DMA is a feature that allows peripherals to directly read and write data from memory, i.e., without involving the CPU every time, improving the system efficiency and performance; they are perfect for periodic tasks or peripherals that constantly need to access memory. A DMA only requires its buffer descriptor to be initially configured with the read and write addresses and other data transfer informations.

Moreover, a DMA block has become a key module in many designs, and its use has already been investigated under radiation conditions (Figure 3.5).

Figure 3.5: SEU corruption of a buffer descriptor



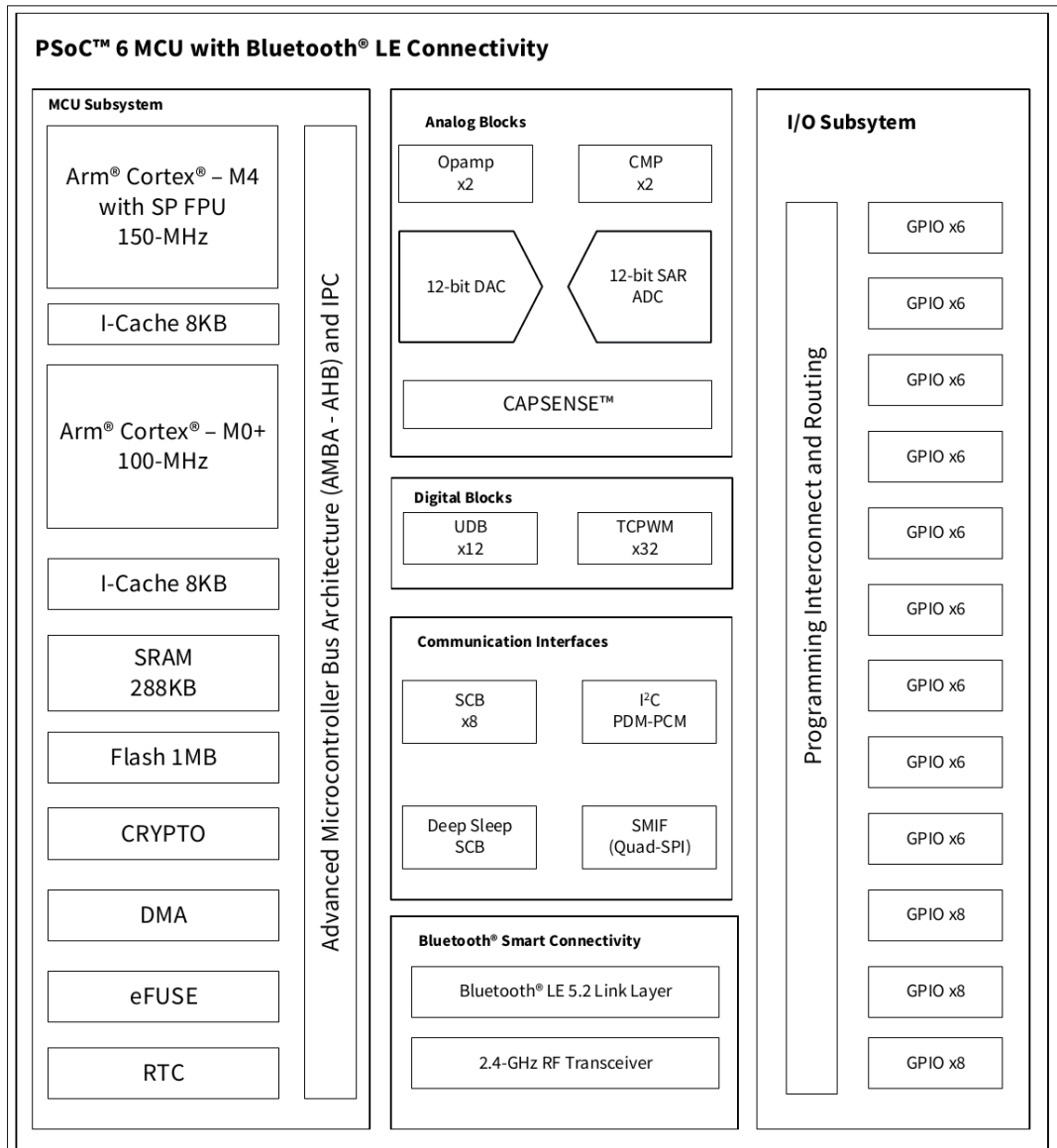
Source: (Portaluri, 2022) [16].

3.1.4 Universal Asynchronous Receiver-Transmitter

A UART, as the name suggests, is a clock-independent data communication protocol that defines how data is structured and transmitted over a serial connection. Both ports must be initially configured with the same parameters in order to ensure a correct data transfer. Some of these parameters include baud rate, stop bits and parity bits.

The UART protocol does not define the voltage and the wiring between the serial ports, these are determined by the physical layer interface such as RS-232, TTL (Transistor-Transistor Logic), or software emulation using bit-banging. Additionally, the UART communication with the PSoC 6 is provided by a USB-UART bridge created by the Kitprog 3, a PSoC 5LP also mounted on the development kit and responsible for programming and debugging the main board device.

Figure 3.6: PSoC 6 features



Source: (Infineon, -) [13].

4 Design Under Test

As mentioned before, the objective of this work is to develop a fault monitoring system in order to identify soft errors in a commercial off-the-shelf (COTS) device. This will facilitate and allow future works to estimate the susceptibility of the SOC in harsh environments by the use of physical or accelerated radiation injection tests. The system was initially designed targeting only SEEs identification, although it may also function for TID or other radiation effects with few or no modifications.

This chapter begins by presenting an overall view of the system and its components; afterward, it describes the functionality of each part and explains how and why some of the design choices were made.

4.1 Monitoring System

The monitoring system is essentially composed of three elements: the main device or device under test, in this case the SOC that will be operating in a radiation environment or under a particle accelerator beam; a second device, which will act as an external watchdog for the main device and serve as an auxiliary driver; and finally, a monitoring computer program, which will manage both devices, coordinate log acquisition and automate the monitoring process.

Figure 4.1: Monitoring system connection schematic.

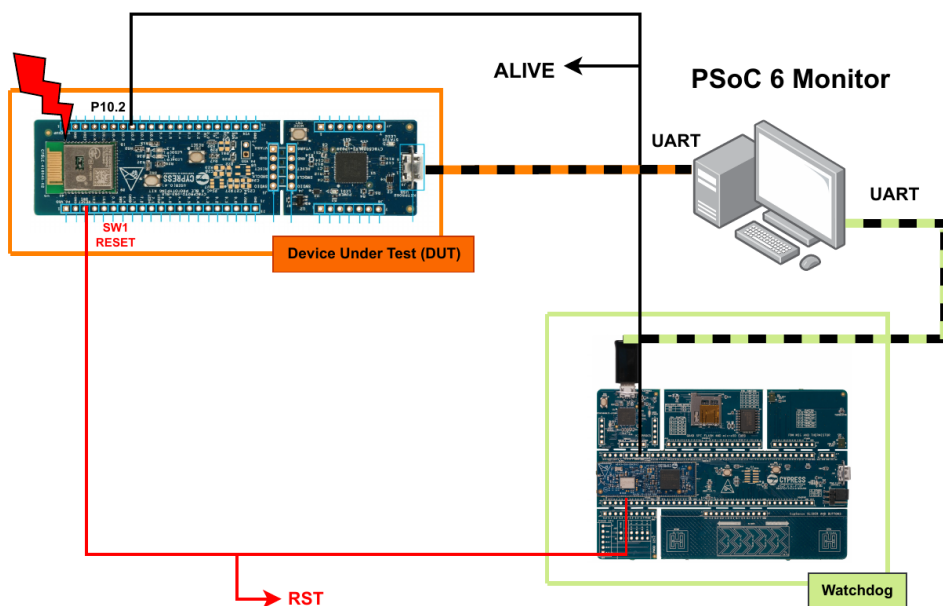
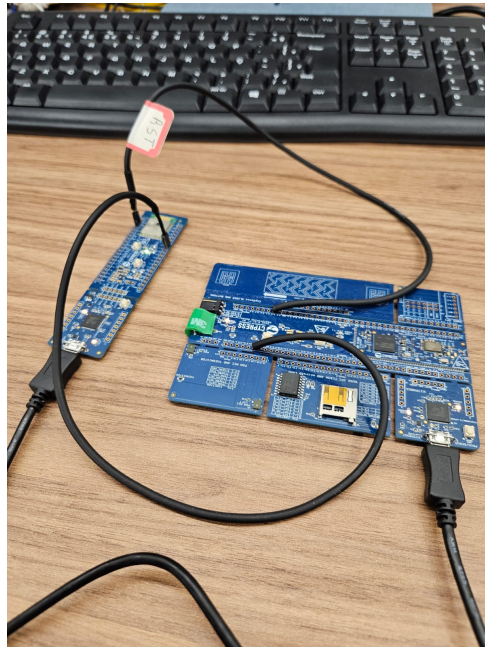


Figure 4.1 represents the connections of the monitoring system, showing both devices connected to a computer via their Micro-USB ports to provide a communication channel and power, along with two additional cables for digital signals. Image 4.2 shows the arranged experimental setup.

Figure 4.2: Experimental monitoring setup.



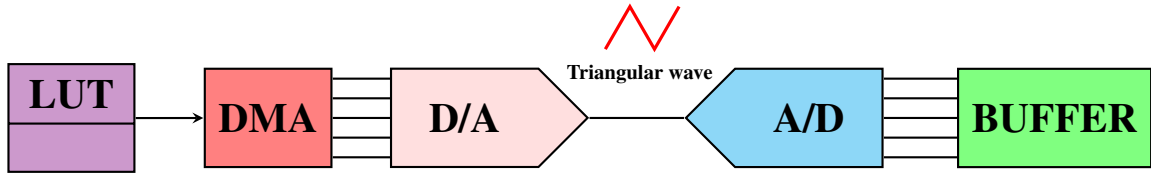
4.2 Main Device

The idea behind this fault detection system is to simulate an environment closely resembling a real situation, limiting the use of only the available peripherals on the SOC –thereby simplifying the setup– and efficiently integrating the majority of the peripherals and their features.

Figure 4.3 summarizes the fault detection system configuration inside the main device. It illustrates the connections of the utilized peripherals and the data flow, starting from the left in the LUT as digital samples, transferred to a DAC via a DMA, becoming an analog triangular wave voltage signal, captured by an ADC and stored in a buffer as digital samples again, before eventually being evaluated by the ARM processor.

Throughout the comparison of the initial signal in the data chain and the signal obtained at the end, it is possible to determine, through direct comparison or by analyzing the signal characteristics, whether or not it was affected during the conversions.

Figure 4.3: Scheme of the fault detection system inside the main device.



Following this specific process, it enables the detection of errors not only in the SOC's digital blocks but also in the analog subsystems. A constant 1 kHz triangular wave is generated using a 500 kHz, 12-bit DAC converter. To achieve this, a LUT stores 500 samples representing one period of the triangular wave, and a DMA is configured to continuously feed these samples to the DAC output register to obtain a precise waveform, since the DMA allows the direct access of memory without the intervention from the ARM processor.

Next, the voltage signal created by the DAC, with a dynamic range of 3.3 V, is read by a 1 MHz and also 12-bit ADC. Even though the maximum converter speed is 1 mega-sample per second, it is only enabled by using an external capacitor or “bypass capacitor”; hence, the actual scan duration takes approximately $13 \mu\text{s}$, and considering $1 \mu\text{s}$ to store the data, the achieved sampling frequency is only 71.42 kHz.

In contrast to the writing process, the read and buffer storage are performed by an interrupt routine inside the processor. The reason for this is that the contents saved to the buffer are not just the acquired data from the ADC; it also includes the time between each sample – measured using a timer – as well as the data written to the DAC output register from the look-up table. Moreover, this buffer is actually divided into three smaller buffers, each of which has a copy of the same information, i.e., there are two backup data storages to also enable the identification of errors in the device's memory.

After 1000 samples are captured to the buffer, the processor begins an error identification algorithm, comparing the difference between each DAC output and its ADC input counterpart, computing the slew rate from the read signal curve, and comparing the three sub-buffer values. Each DAC/ADC comparison, as well as the slew rate, is evaluated based on characteristic values pre-established during a “training phase” in a safe environment, where the expected values and tolerance values for the specific setup are determined and set respectively.

The slew rate of the triangular wave is calculated only by the absolute difference between two samples, the division operation is simplified since the time difference between samples is approximately constant at all times. Although, the time difference is still verified

separately for eventually errors that might occur with the timer module.

Furthermore, this buffer processing time, which is directly related to the buffer size, can be seen as a dead zone or blind spot for possible errors in the system, since the data from the converters are ignored during this period. Therefore, there is an exclusive timer to count the total monitoring time, which is paused at the beginning of this processor's routine and restarted at the end.

If an error is detected, it is flagged in a register that accounts for all the possible error types being verified, and the buffer is sent via UART to the monitoring program, where it will be logged to a file for further inspection and analysis. Each buffer is divided into 10 smaller buffers that will be transmitted in packets containing a header, payload and checksum field. Additional information about the packet format will be discussed later in the Monitoring Software section.

Finally, after all data has been sent, the device is rebooted using its internal watchdog to guarantee the correct operation of the system for future detection routines (assuming that the captured fault was a soft error).

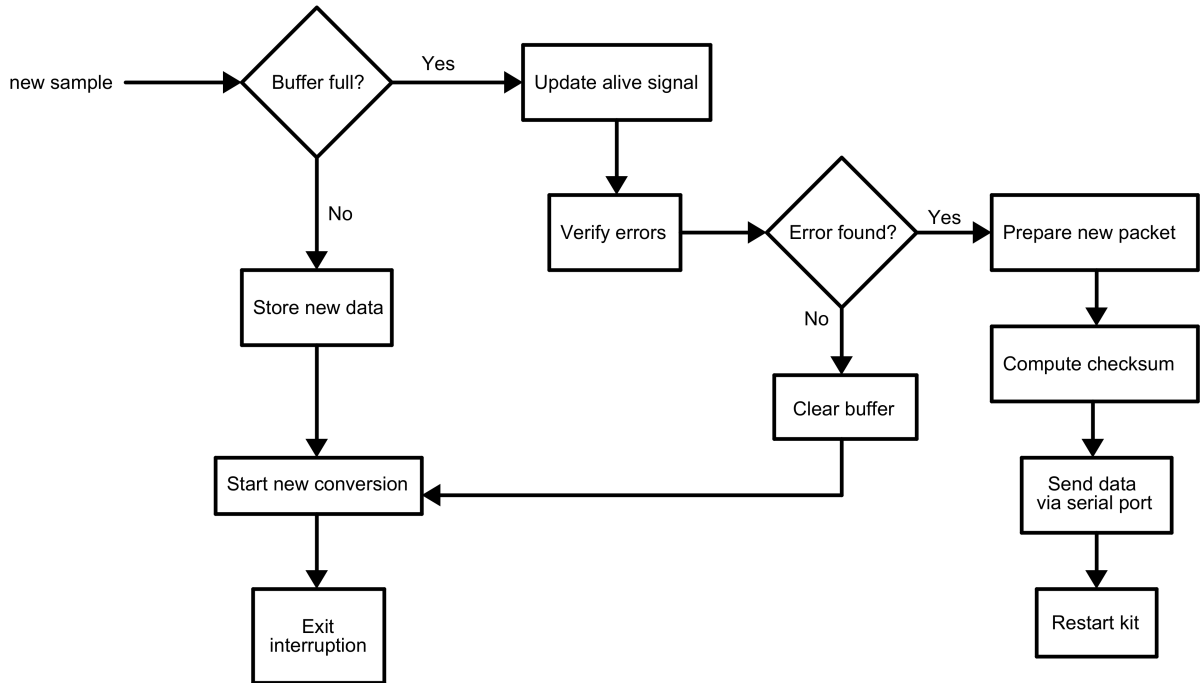
This methodology was inspired in an older work, available at (Siqueira, 2022) [17], where it was studied the PSoC 6 reliability to electromagnetic interference; however, a much simpler system was developed, adopting different design choices –e.g., a sinusoidal wave of 1 Hz– since the overall goal was not the same.

In addition, the current method only works because the expected signal at the end of the data chain is known beforehand, or at least some of its characteristics. Related works, as in (González, 2021) [18], which uses an older SOC technology (PSoC 5), propose different techniques employing redundant systems with spatial and temporal voters. In this case, it presented a good alternative due to the hardware capabilities, containing three different ADCs (one 74 ksps Sigma-Delta, one 74 ksps SAR and another 740 ksps SAR). However, in many cases such as in the PSoC 6, these hardware redundancy approaches may not be available. Therefore, it is essential to investigate new methods to withstand and identify radiation errors.

Figure 4.4 summarizes the interrupt routine when new data is sampled by the ADC. Another important feature of this system, not yet mentioned, is the main device alive signal; it serves as a status check, indicating that the system is running as expected. This alive signal is actually divided into two signals: the first one transmitted via a digital pin to the external watchdog, which provides a quick acknowledgment that the ARM interrupt service routine is working correctly; and the second one is sent via the serial port as an ASCII pattern directly to

the monitoring software, indicating its accurate function.

Figure 4.4: Main device processor interrupt routine flow diagram.



Also, because this system does not retrieve or rectify the correct samples in case of an error in the data conversion chain, it does not mitigate the radiation effects like a TMR system or ECC memory. Nevertheless, it can instruct the system that the information collected cannot be trusted. In reality, no system is fully protected to the radiation effects; they are designed to be sufficiently tolerant for a specific application, since their protection is directly related to project costs.

Besides the data converters frequencies, which were chosen to work at their maximum rates, the triangular wave frequency, the buffer size and other design choices were empirically determined by the assistance of experimental tests. So, taking into account an effective 71.42 kHz sampling rate and a buffer size of 1000 samples, the total buffer time is 14 ms; then, about 14 periods from the curve can be observed in a single buffer, since the triangular wave frequency is 1 kHz.

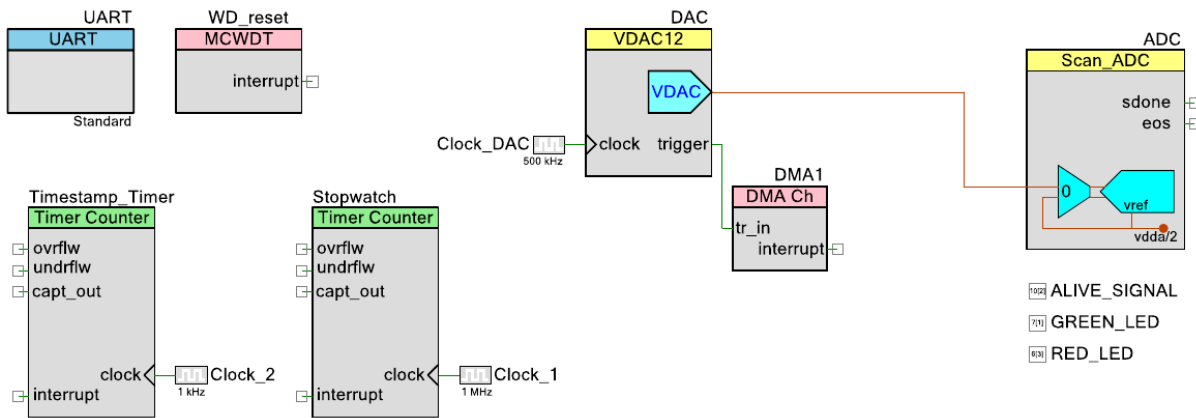
Therefore, a window of 14 periods provides great flexibility in observing the effects an error may cause to the signal and enables the use of a higher nominal sampling rate in the future. Moreover, the triangular waveform is perfect for determining its slew rate, as its magnitude should remain constant far from the curve's extremities.

The SOC was programmed using a development tool or IDE called “PSOC Creator”

from Infineon. This program provides a graphical user interface to connect, arrange and configure the available peripherals for the target PSoC, for which part of the code is auto-generated. This facilitates the configuration of the blocks and speeds up the design process at the beginning.

Figure 4.5 shows how the fault detection system translates to the PSOC Creator user interface. The final design choice worth noting is the use of only one of the dual CPUs present in the SOC; only the ARM Cortex M4 is programmed for design simplicity.

Figure 4.5: Block diagram in PSOC Creator.

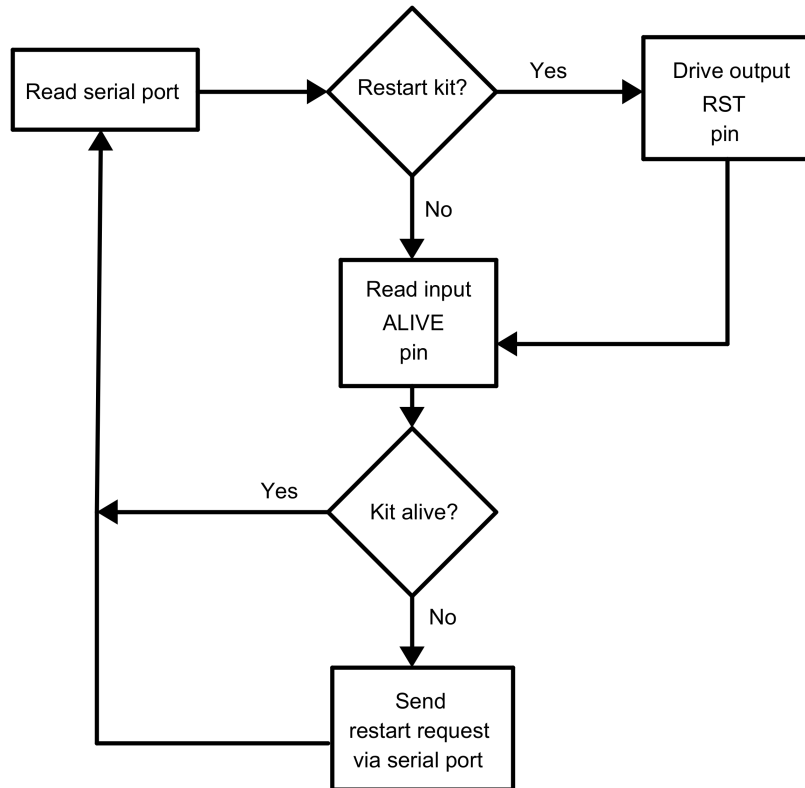


The code –developed in C programming language– for the main device (PSoC 6) fault detection system is available in the following GitHub repository (Fabbris, 2024) [19].

4.3 External Watchdog

It is important to first clarify that other devices could have been used as an external watchdog, though, for convenience, it was chosen a different PSoC 6 version mounted in another Cypress development kit (CY8CPROTO-062-4343W). To replace the current watchdog hardware with another, the only requirements would be an UART connection, two external pins and a processing unit capable of running the logic described in Figure 4.6.

Figure 4.6: External watchdog routine flow diagram.



Even though the external watchdog is responsible for driving the development kit reset pin to restart the PSoC 6, it is not responsible for making the decision, since it just transmits the information whether or not the code has been executing correctly and leaves the algorithm in the monitoring program as the decision maker.

The external watchdog is not mandatory, although it automates the experimental test process, as it enables the main device management through the computer software, considering that some tests can last hours or even days.

For this secondary device, the software used to program it is called “ModusToolBox”, which is different from the main device because the target PSoC 6 version is not supported by the PSOC Creator. This tool does not have a similar graphical user interface, so it can be a little cumbersome or not friendly for beginners, although there are many examples on the internet and documentation explaining how to configure the user desired modules. For the external watchdog routine, only timers and pins were needed to be configured.

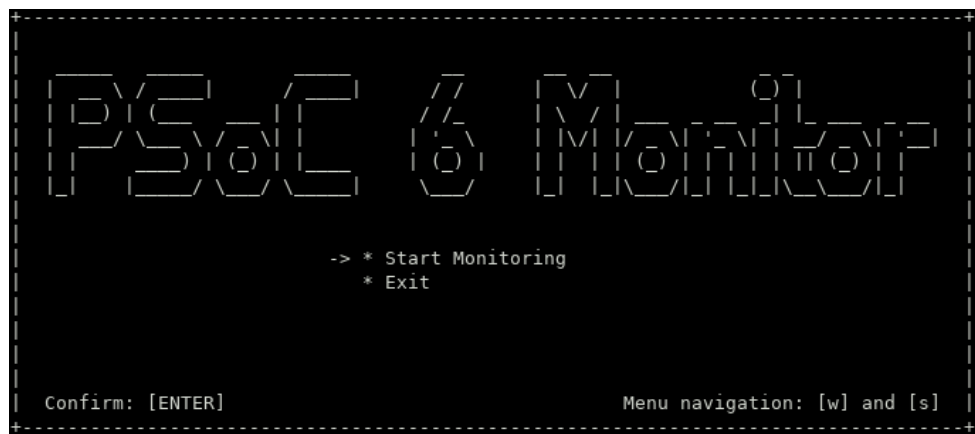
The code –also developed in C programming language– for the secondary device (PSoC 6) external watchdog system is available in the following GitHub repository (Fabbris, 2024) [20].

4.4 Monitoring Software

As mentioned above, some experimental tests by physical radiation injection can last long time periods. Hence, the “PSoC 6 Monitor” was created to manage these accelerated tests and enable them to be seen as simple “plug and play” systems after the serial ports from both devices are configured. The idea is that anyone should be able to perform the experiment, the test operator just needs to follow a simple user guide to setup the system and it is “ready to go”, there is no need for intervention.

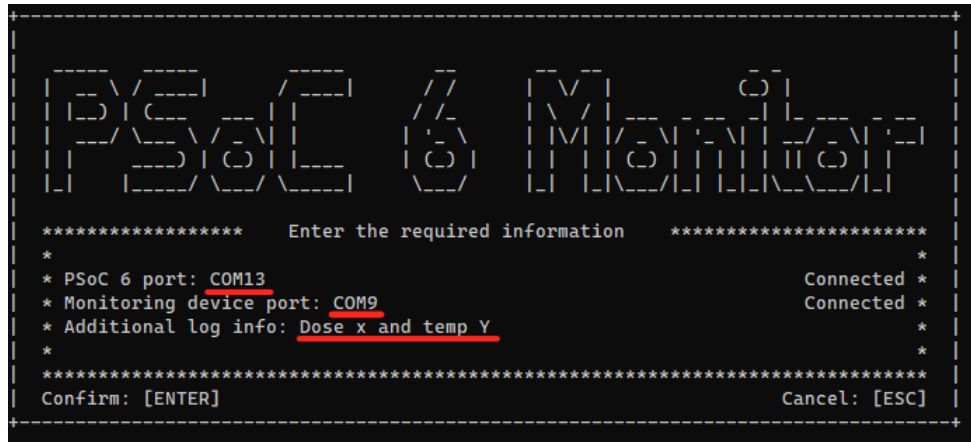
The program was developed for both Windows and Linux operating systems, expanding the options for computers to run the program in the experiment environment. Image 4.7 shows the initial menu for the PSoC 6 Monitor.

Figure 4.7: PSoC 6 Monitor initial menu.

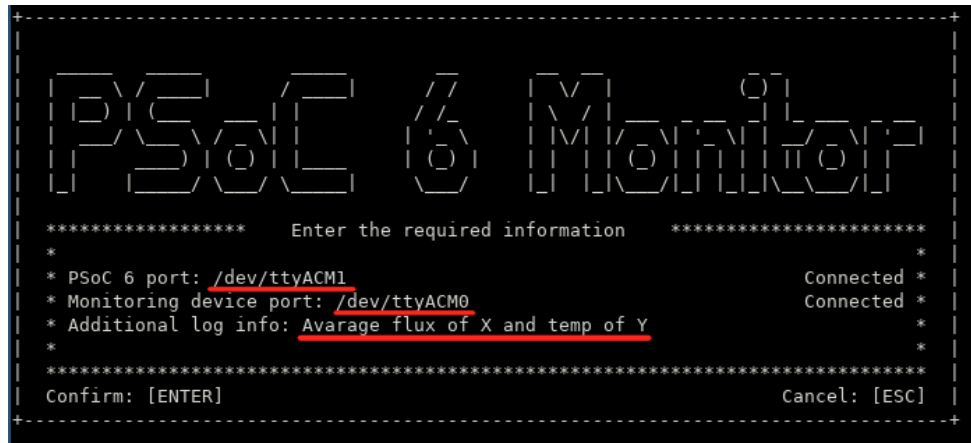


By entering the option “Start Monitoring”, the program will lead the user to its serial port configuration menu, where the operator will be prompted to inform the program both devices serial port names, as well as some optionally additional information about the new monitoring session, which will be saved to the log with the captured buffers. The described is illustrated by Figure 4.8, for Windows and Linux respectively.

Figure 4.8: PSoC 6 Monitor serial port configuration.



(a) Connecting devices serial ports on Windows.



(b) Connecting devices serial ports on Linux.

A new session will be initiated as soon as the user presses the “ENTER” key on the keyboard – considering that all the devices were recognized and successfully connected. At the beginning of a new session, a new log file is created inside the “log” folder at the same path where the application was executed. Each file is categorized by its creation timestamp in seconds, representing the day and hour accordingly to the epoch of the system.

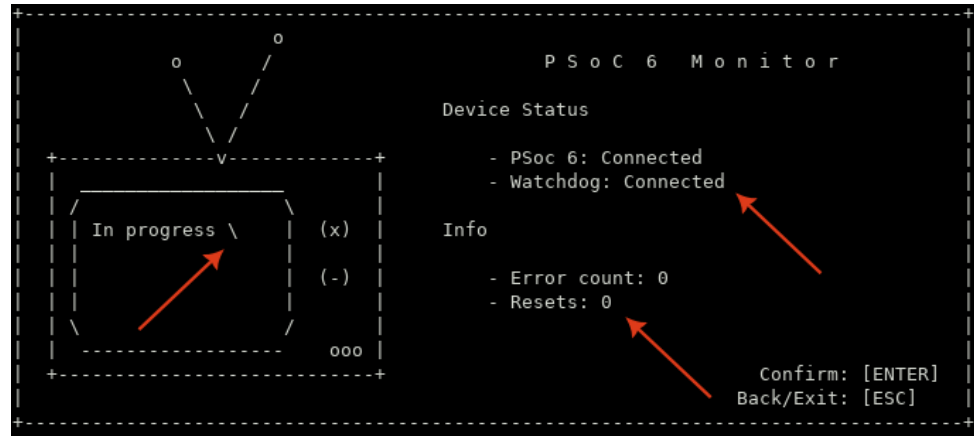
Figure 4.9 demonstrates the program screen when a new session is started, indicating that no buffer has been received yet (Error count equals zero), and no intervention by the monitoring software has been made (Resets equals zero).

The software will continually manage the fault detection system, logging new buffers if an error is found and resetting the main device in case the UART connection is lost or the interruption routine in the PSoC 6 is not being executed.

Furthermore, at the beginning of each session, the program sends a reset command to

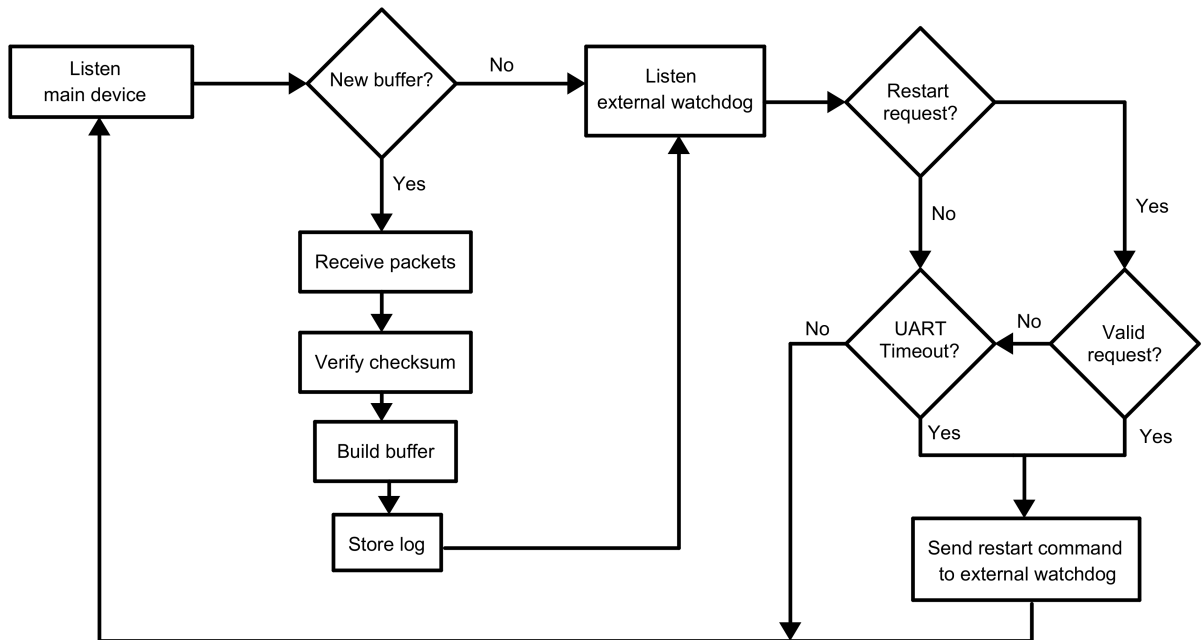
the external watchdog to restart the main device, therefore, it resets the device state and status, and the monitoring timestamp sent with each buffer, which indicates the total monitoring time and accounts for the buffer verifications pauses or dead zones as mentioned before.

Figure 4.9: PSoC 6 Monitor monitoring menu.



The algorithm running behind the monitoring menu is described by the diagram from Figure 4.10.

Figure 4.10: Monitoring software routine flow diagram.



The PSoC 6 Monitor can be represented as the commander or the maestro which orchestrates the entire system. It starts by listening to the main device serial port, searching for new packets. In case it does receive a new buffer packet, then the program initiates a log

acquisition process by getting the computer timestamp, decoding each of the next 10 packets, verifying their checksum and rebuilding the buffer to its original size.

Every packet is formed by a header, payload and checksum field, Table 4.1 represents its format.

Table 4.1: Buffer packet format.

8 bytes	700 bytes	2 bytes
Header	Payload	Checksum

Dividing the buffer in smaller packets ensures that not all data is lost in case of some communication error during the transmission, also it improves the monitoring software performance, since the program only runs in a single thread, and requires smaller buffers at the reception. Additionally, it enables for future communication improvements as an acknowledgement system for example.

Table 4.2 describes the three fields from the packet header; the “Offset” and “Size” cells are indicated in bytes. The timestamp sent with each packet is different from the operational system timestamp, it represents the total monitoring time or the elapsed time until an error is found with a precision of 1 ms.

Table 4.2: Packet header fields.

Offset	Size	Name	Description
0	2	PCKT_ID	ASCII packet identifier
2	2	BUF_OFST	Buffer offset or packet sequence
4	4	TIMESTAMP	Monitoring time

For the payload section, Table 4.3 summarizes its fields descriptions. Considering a buffer size of 1000 samples divided into 10 packets, each packet has 100 samples from the ADC. Although, as discussed earlier, the information stored has also the output from the DAC and the conversion time captured by a timer. The error descriptor register, determined at the buffer verification routine, is also attached to the beginning of the payload, providing the error description that was identified by the system.

Table 4.3: Packet payload fields.

Offset	Size	Name	Description
0	1	ERROR DES	Error type descriptor
1	2	DELTA_T	Time difference between each sample in μs
3	2	ADC_IN	ADC input or read sample
5	2	DAC_OUT	DAC output or written sample

Table 4.4 shows the definition of each bit from the Error descriptor register. It serves as a quick check for the received data and indicates where the possible error was caught.

Table 4.4: Error type descriptor register.

Bits	Name	Description
7	BCKP_ADC_IN	ADC input mismatch in backup buffers
6	BCKP_DAC_OUT	DAC output mismatch in backup buffers
5	BCKP_DELTA_T	Time difference mismatch in backup buffers
4	DT	Time difference outside tolerated range
3..2	-	Reserved for future use
1	SR	Slew rate outside tolerated range
0	DX	Written and read difference outside tolerated range

The checksum is the last field from the packet, it is used as a simple verification mechanism to make sure the received data is in order and the UART module from the main device PSoC 6 is operating correctly.

Figure 4.11 illustrates a file log, where one buffer was received during a session of approximately one hour. All the session status is also stored to the file, every new entry is logged with a timestamp, providing a timeline of the occurred events. In this example, where the system was under a design verification test, the connection from the serial port is initially lost, then the program tries its first reset attempt and the main device connection returns.

Figure 4.11: Information stored in a log file.

```
*****
* @filename: log_1729457875_0.txt
* @brief: This file is intended to store information about PSoc6 radiation
*          tests
* @info:
*
*****
@t (1729457893) psoc6 connection DOWN
@r (1729457893) DUT reset attempt #1, req dsc: 1
@t (1729457894) psoc6 connection UP
@B0, 15288 - received at (1729457911) Sun Oct 20 17:58:31 2024
received packets: 10, checksum error: false, timeout error: false
1460    1459    13      0
1344    1344    13      0
1230    1230    13      0
1114    1115    13      0
1000    1000    13      0
884     885     13      0
.
.
.
1687    1574    13      1
*****
* @Session summary:
*
* - Start time: 1729457875
* - End time: 1729461622
* - Elapsed minutes: 62.45
* - Received buffers: 1
* - Received packets: 10
* - Resets: 1 (core hangs: 0, serial connection: 1)
* - Packet checksum errors: 0
* - Monitor device lost connection: false
*
*****
```

Every buffer logged to the file also informs if a checksum error or a timeout packet error happened, and how many packets from this buffer were indeed retrieved. At the end of the file, a small summary from the session is printed, notifying the amount of errors detected. Moreover, if the log passes a certain limit, its buffers will be divided into multiple files, avoiding big records.

Right after “B0” (Buffer 0) the timestamp can be found, representing a monitoring duration of only 15 seconds because the device had just been restarted. The first column of the buffer stands for the ADC value, followed by the DAC output, time difference and error descriptor. In this situation, the error descriptor equals one, meaning that a “DX” fault was detected.

Another important feature from this system is the reset algorithm. After listening to the external watchdog and receiving a restart request, the program examines the request. For example, if the main device just finished sending a new buffer to be logged, it will auto-restart

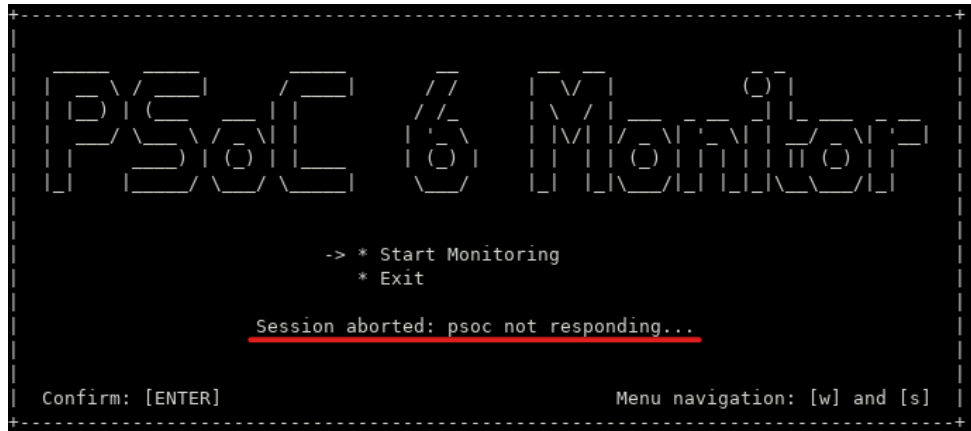
itself, which will take a brief moment; although, because the external watchdog does not know this in advance, it will accuse that the main device has stopped working properly and send a restart request to the monitoring software.

Contrary to the digital pin alive signal, the serial port alive is only used to verify whether or not the communication system is still intact, and has a much greater timeout. The timeout for the alive signals from UART and the digital pin are about 10 s and 100 ms respectively.

Considering a valid request from the auxiliary device, there is one more step before sending the restart command. The program cannot constantly keep restarting the main device if it does not immediately respond. Instead, it will check whether it has recently attempted to restart the device and will wait a while before trying again.

The program will consecutively try to revive the main device 7 times, if none of these attempts succeed, then the session will be aborted (Figure 4.12). A cooldown time between each attempt is gradually incremented, starting at 5 seconds, increasing to 10, 30...300 seconds and so forth. Therefore, even though there is a valid restart request, the cooldown needs to be respected before another restart command is issued.

Figure 4.12: PSoC 6 Monitor session aborted.



Similar works usually opt for simple serial consoles like Putty, however, in these situations manually intervention may be needed multiple times and data organization may be neglected. The introduced system can also be used stand-alone by adjusting some configuration registers on the code, although it would be a “single-instrument orchestra without a maestro”.

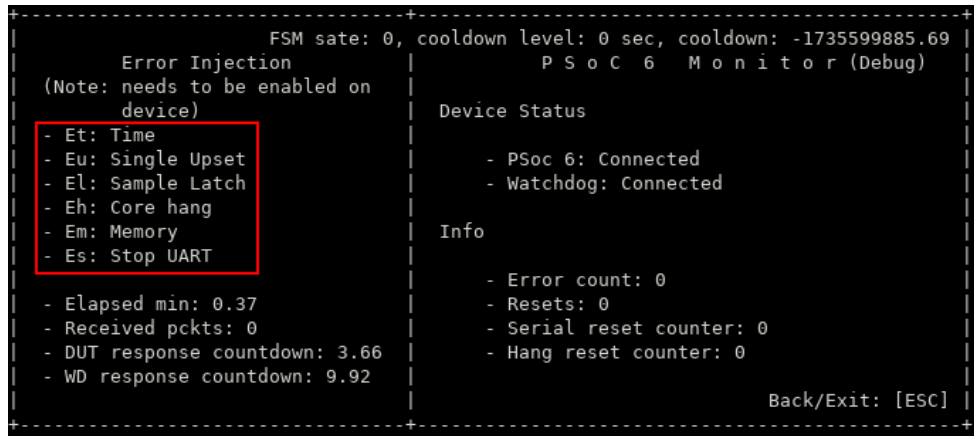
The code –developed in C programming language– for the monitoring software is available in the following GitHub repository (Fabbris, 2024) [21]; a user guide with more

information about the system is also provided.

5 Design Validation

In order to validate the proposed fault detection system, soft errors were emulated via the monitoring software working as a debug platform. This debug feature works as an optionally module in the main device and must be enabled before. Figure 5.1 depicts the debug menu from the monitoring software that will be available during the session when the key sequence “DM” (Debug Mode) is pressed in succession.

Figure 5.1: PSoC 6 Monitor debug menu.



```

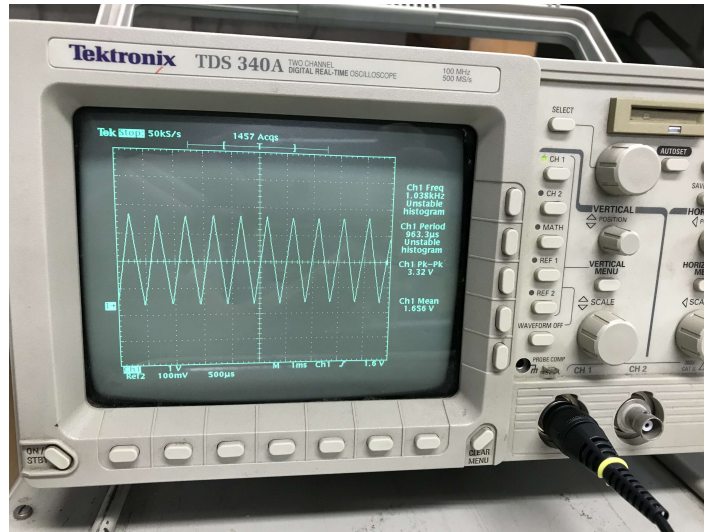
+-----+
|           FSM state: 0, cooldown level: 0 sec, cooldown: -1735599885.69 |
|           P S o C 6   M o n i t o r (Debug)                         |
|           (Note: needs to be enabled on                                |
|           device)                                                 Device Status          |
|           - Et: Time                                         - PSoc 6: Connected    |
|           - Eu: Single Upset                               - Watchdog: Connected |
|           - El: Sample Latch                                Info                  |
|           - Eh: Core hang                                 - Error count: 0        |
|           - Em: Memory                                    - Resets: 0            |
|           - Es: Stop UART                                - Serial reset counter: 0 |
|           - Elapsed min: 0.37                            - Hang reset counter: 0 |
|           - Received pkts: 0                           Back/Exit: [ESC]      |
|           - DUT response countdown: 3.66               +-----+
|           - WD response countdown: 9.92
+-----+

```

The debug platform allows the emulation of some of the consequences that a SEE may generate on the system, which were already recognized in previous works using a 130 nm PSoC 5 (González, 2021) [18]. By pressing the key sequence “E” followed by one of the letters in the error injection menu in Figure 5.1, a command via the serial port will be transmitted and the main device will trigger the logic behind the desired error, therefore, this can be seen as a software error injection.

The triangular wave frequency and waveform were also verified using a oscilloscope and temporarily connecting the DAC output to an external pin. Figure 5.2 shows the generated wave.

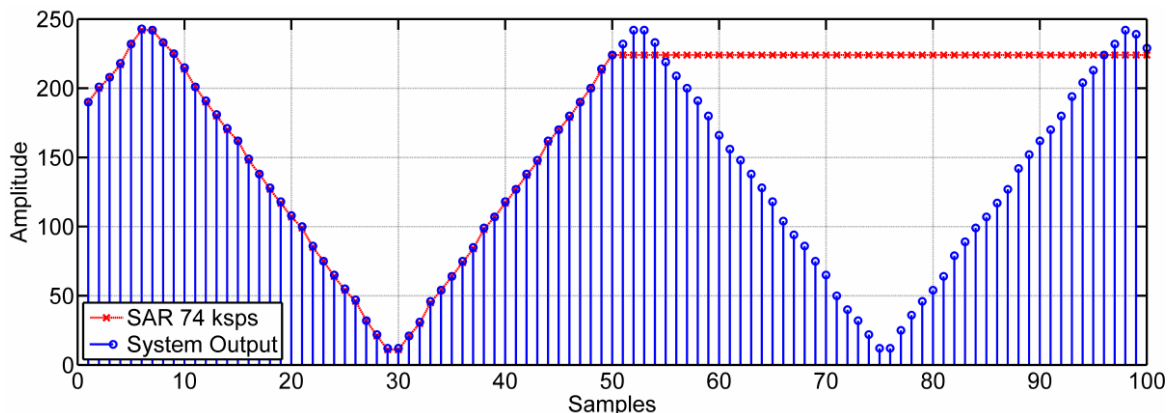
Figure 5.2: Oscilloscope at the DAC output.



Two heavy ion campaigns were performed with the PSoC 5 at the 8UD Pelletron Accelerator in São Paulo, targeting the device with an oxygen-16 ion beam. The SOC was irradiated at a zero angle with its top package removed, producing an effective LET of 5.5 Mev/mg/cm² at the silicon's active region. Furthermore, the average flux in each campaign and their duration were 350 particles/s/cm² and 246 min, and 430 particles/s/cm² and 288 min, respectively (González, 2021) [18].

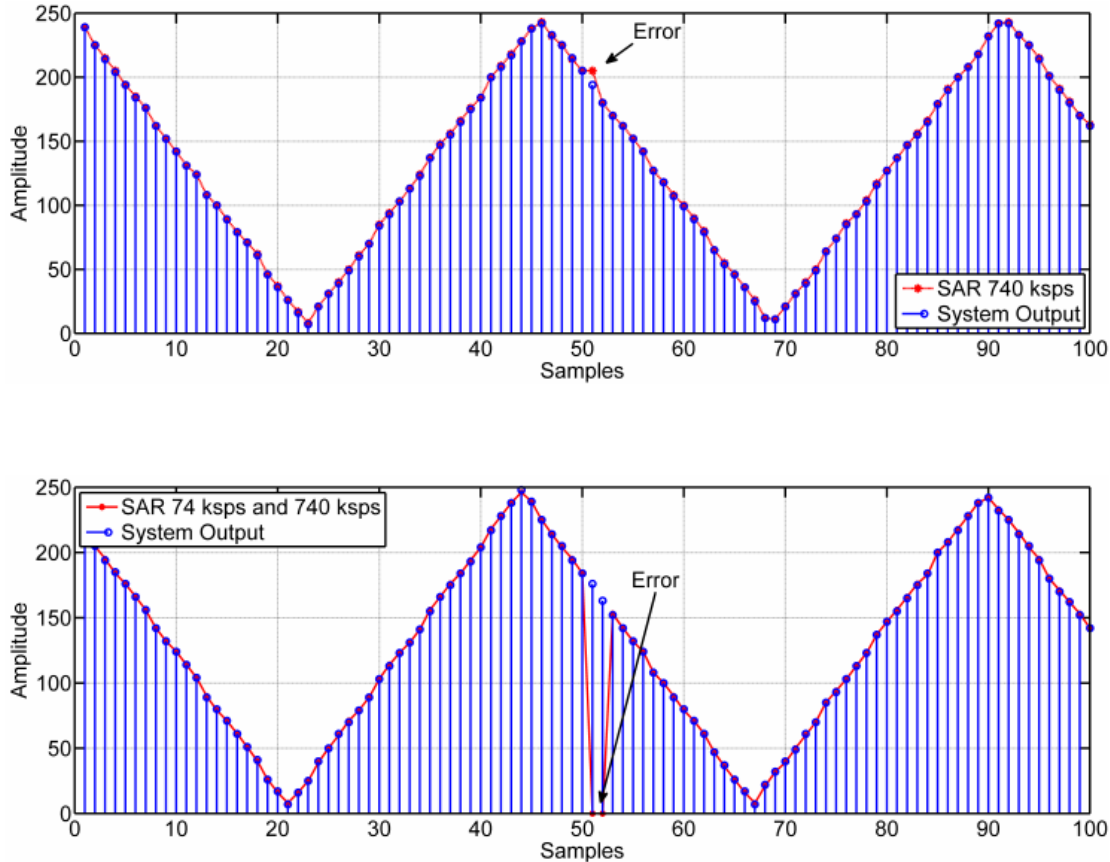
During both heavy ion experiments, 353 errors were observed, with 255 being system hangs and 98 being SEU or SEFI on the converters. Some of these SEU and SEFI discovered and represented by Images 5.3 and 5.4 were reproduced in the PSoC 6 as a validation method throughout the “Eu” and “El” commands.

Figure 5.3: PSoC 5 SEFI example.



Source: (González, 2021) [18]

Figure 5.4: PSoC 5 SEU example.



Source: (González, 2021) [18]

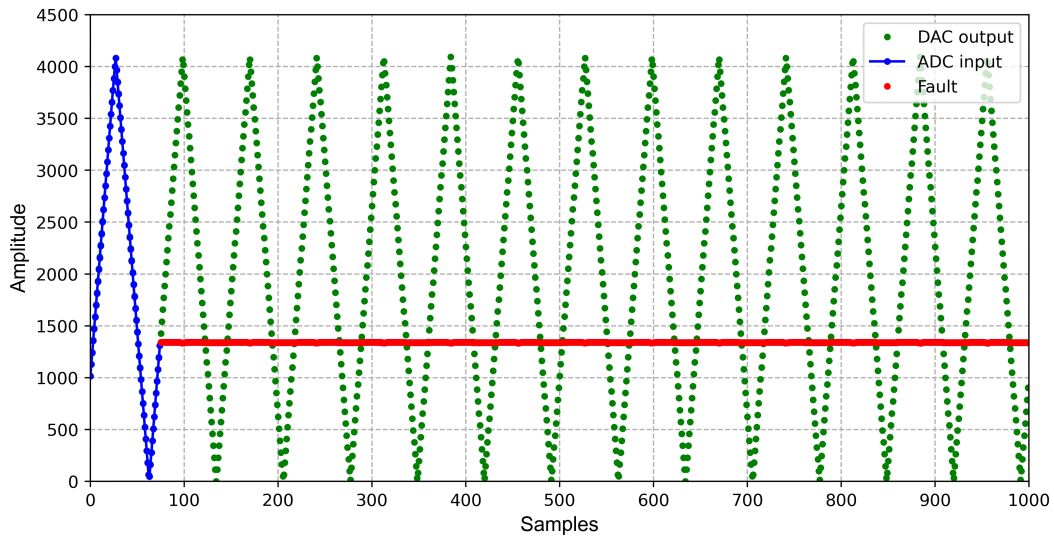
When “Eu” or “El” are pressed, the main device will bypass the DMA data and overwrite the DAC output register, hence, temporarily modifying the expected input at the ADC. In the case of “Eu”, only a pre-selected single bit from the 12-bit DAC output word is flipped, simulating a SEU on the mixed-signal peripherals. If “El” is selected, then the current data from the output DAC register will be held until the device is restarted, simulating a SEFI from the converter blocks.

After receiving the debug buffers, they can be plotted using the available script for buffer handling and data visualization in Python, present in the same repository from the PSoC 6 Monitor program. Data plots in Figures 5.5 and 5.6 demonstrate the reproduction of the effects seen with the PSoC 5, verifying the correct functionality of the proposed error identification system.

As commented before, the expected values for the read triangular wave and its slew rate are determined during a “training phase” or calibration routine, where the main device will

continuously evaluate the difference between the written and read samples and the slew rate of the curve, and always check for new maximum and minimum reference values, defining an operation range for the device. When the operation range is determined, a tolerance value is also added as a safety margin; for this system, a 5 LSB margin was considered as the tolerance value.

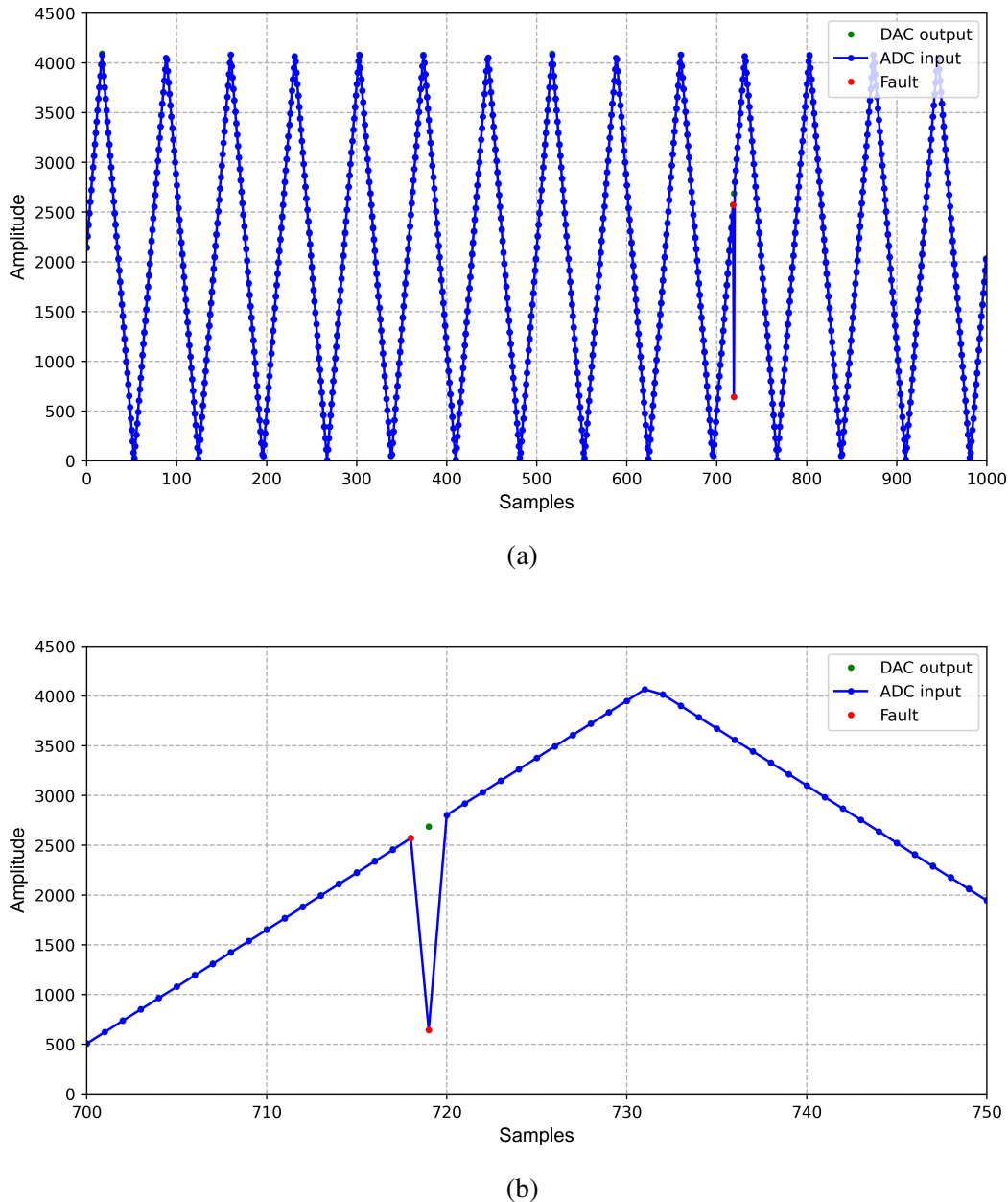
Figure 5.5: PSoC 6 SEFI emulation through debug platform.



Due to the square wave characteristic curve from the slew rate of a triangular wave and a finite sampling rate from the ADC, the tolerated values for the slew rate will accept a zero or approximately zero value. This can be understood by glancing at the read triangular wave peaks, where the captured samples form a “flat-top” (Figure 5.6b). For this reason, errors as SEFI in the plot above (Figure 5.5) were not identified as “SR” faults, because the same sample is held by the DAC and the slew rate will translate to zero or approximately zero.

Therefore, for this configuration, i.e. a triangular wave and sampling rate of 71 kHz, the mechanism comparing the written and read samples is essential for identifying these type of errors.

Figure 5.6: PSoC 6 SEU emulation through debug platform.



The most sensitive bits from the 12-bit word registers at the converters are the most significant bits. The reference values and tolerance values for the written and read data comparison account for the digital-to-analog and analog-to-digital conversion errors from the converters. Therefore, with this setup, approximately the four least significant bits from these registers will not be detectable in case of bit flips.

SEUs in the buffer memories will be identified by the triple buffer redundancy, and can be emulated by pressing “Em”, which will flip a bit from both backup buffers data. Moreover,

the timer used to measure the time between each sample can also be tested typing “Et”, which will purposefully add a delay inside the processor interrupt routine.

The majority of the errors observed in the PSoC 5 are not related to the converters, they are system hangs due to the processor or the UART communication. Thus, it is crucial to also simulate the system behaviour in these type of situations, this can be achieved by using the “Eh” and “Es” sequences. By sending an “Eh” command, the processor interrupt routine will be halted by an infinite loop, forcing the external watchdog to accuse an error to the monitoring software, which will command the watchdog to restart the main device. This can be seen as an increment in the “resets” and “hang reset counter” indicators at Figure 5.1.

When pressing “Es”, the system will continue to operate normally, although, the UART alive signal will be bypassed, ultimately causing the monitoring program to accuse that the serial port was disconnected after its timeout and commanding the external watchdog to restart the device. This also can be seen as an increment in the “resets” and “serial reset counter” indicators. Furthermore, every reset attempt by the program is recorded into the log file (Figure 4.11).

The slew rate computation serves as a great post buffer analysis, after all the data is captured to a buffer using a DMA at the ADC output for example. Although, its use aside the comparison between the ADC and DAC samples needs to be further investigated in future works.

No radiation tests have been performed yet; however, results are expected in the next few months, as a system kit has already been sent to a neutron facility for the system’s first physical irradiation experiment. Therefore, future works will be needed to evaluate this test results and the system overall performance, and to improve and adjust the system for unidentified bugs. Compared to the PSoC 5, it is expected a grater impact in the PSoC 6 device due to SEE, since its newer 40 nm technology process.

Finally, one of the system “flaws”, that may also be tackled in future works, is that, in most cases, it is not possible to identify in which state from the data chain the data was corrupted, as the captured value from the ADC may have been changed before it is written by the DAC, at the DAC or at the ADC for example.

6 Conclusion

An error identification system was developed using three main elements: the Device Under Test, an External Watchdog and a Management Program Interface. Each part has proven essential for the desired purpose of detecting Single Event Effects and automating experimental tests that can last hours or even days.

Numerous tests were performed with the system, some totaling more than 12 hours uninterrupted sessions. In many of these experiments, only the stability of the system was verified, i.e., no fault emulation or interaction with the debug platform was applied. In others cases, all listed debug stimuli described were injected to ensure the correct response of the system during different time periods.

The validation of the soft error identification system was successful, as the system demonstrated the expected behaviour during the debug sessions, identifying bit-flips or SEUs, and held samples by the converters or SEFIs. Additionally, system hangs and the loss of the communication channel were handled by the external watchdog and monitoring software.

The next step planned for future work is to conduct physical radiation experiments utilizing different sources, proving the correct operation of the identification system and collecting data to evaluate the susceptibility of the device for different types of radiation.

Finally, adjustments and improvements for the system may be needed in the future, the computation of the slew rate requires further investigation. The future results must also be compared with the previous ones obtained for the PSoC 5, checking if the device reliability has decreased for SEE due to the newer technology process node. New mitigation techniques may be carried out to allow the device to withstand new radiation environments, not just identifying the errors but also recovering the corrupted data. If an external bypass capacitor is added to the ADC, higher sampling frequencies will be possible, enabling the use of a voting system to capture the same data at different time periods for example.

References

- [1] Tiago R. Balen. “Efeitos da radiação em dispositivos analógicos programáveis (FPAAs) e técnicas de proteção”. In: *Doctoral Thesis in Electronic Engineering, Federal University of Rio Grande do Sul* (2010). URL: <https://lume.ufrgs.br/handle/10183/27254>.
- [2] S. Mukherjee. *Architecture Design for Soft Errors*. Elsevier, 2008.
- [3] R. Baumann and K. Kruckmeyer. *Radiation Handbook for Electronics*. Texas Instruments, 2019.
- [4] A. P. French and E. F. Taylor. *An Introduction to Quantum Physics*. New York, W. W. Norton & Co., 1978.
- [5] P. P. Urone and R. Hinrichs. *College Physics*. OpenStax, 2020.
- [6] C. J. Moses R. A. Serway and C. A. Moyer. *Modern Physics*. Thomson Learning, 2005.
- [7] J.W. Howard and D.M. Hardage. *Spacecraft Environments Interactions: Space Radiation and Its Effects on Electronic Systems*. NASA, 1999.
- [8] Goddard Space Flight Center NASA. *What are the Van Allen Belts and why do they matter?* -. URL: <https://science.nasa.gov/biological-physical/stories/van-allen-belts/>. Accessed in: December 2024.
- [9] M. Nicolaidis. *Soft Errors in Modern Electronic Systems*. Springer, 2011.
- [10] Andreas Horn. *Single Event Effects - The Achilles heel of modern aerospace electronics*. 2021. URL: <https://www.engineeringpilot.com/post/single-event-effects-the-achilles-heel-of-modern-aerospace-electronics>. Accessed in: December 2024.
- [11] Fan Wang and Vishwani D. Agrawal. “Single Event Upset: An Embedded Tutorial”. In: *IEEE - 21st International Conference on VLSI Design* (2008).
- [12] Infineon. *Introducing the Infineon - PSoC 6 Microcontroller Family*. -. URL: <https://www.infineon.com/cms/en/product/promopages/20-years-of-psoc/psoc6-technical-look/>. Accessed in: January 2025.
- [13] Infineon. *PSoC 6 Family Documentation*. -. URL: <https://documentation.infineon.com/psoc6/docs/rkg1651145413836>. Accessed in: January 2025.

- [14] Behzad Razavi. “A Tale of Two ADCs - Pipelined Versus SAR”. In: *IEEE SOLID-STATE CIRCUITS MAGAZINE* (2015).
- [15] Behzad Razavi. “The Current-Steering DAC”. In: *IEEE SOLID-STATE CIRCUITS MAGAZINE* (2018).
- [16] A. Portaluri. “Radiation-induced Effects on DMA Data Transfer in Reconfigurable Devices”. In: *IEEE 28th International Symposium on On-Line Testing and Robust System Design (IOLTS)* (2022).
- [17] Douglas A. S. Siqueira. “Avaliação de efeitos e formas de mitigação de interferência eletromagnética em um conversor analógico-digital SAR de um SoC programável”. In: *Electronic Engineering Graduation Thesis, Federal University of Rio Grande do Sul* (2022). URL: <https://lume.ufrgs.br/handle/10183/245875>.
- [18] Carlos J. González. “Testing a Fault Tolerant Mixed-Signal Design Under TID and Heavy Ions”. In: *Journal of Integrated Circuits and Systems* (2021). DOI: <https://doi.org/10.29292/jics.v16i3.567>.
- [19] Eduardo Fabbris. *PSoC 6 Error Detection Github Repository*. 2024. URL: https://github.com/eduardofabbris/error_detection.git.
- [20] Eduardo Fabbris. *External Watchdog Github Repository*. 2024. URL: https://github.com/eduardofabbris/external_watchdog.git.
- [21] Eduardo Fabbris. *PSoC 6 Monitor Github Repository*. 2024. URL: https://github.com/eduardofabbris/psoc_monitor.git.